Article

Cell Reports

Uncoupling Malt1 Threshold Function from Paracaspase Activity Results in Destructive Autoimmune Inflammation

Graphical Abstract

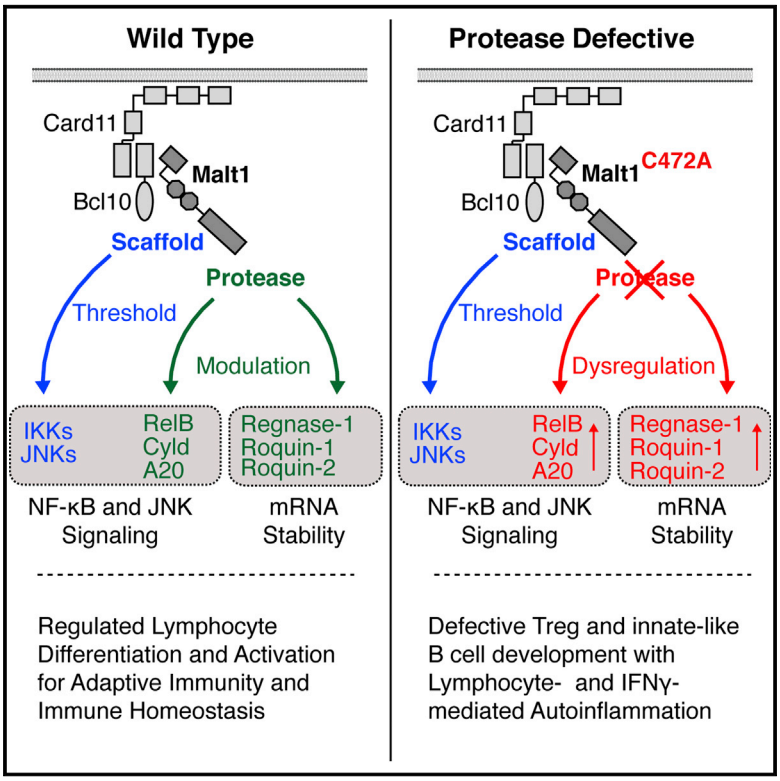

Highlights

The Malt1 scaffold and Malt1 paracaspase activity have differential functions in vivo

Malt1 protease activity is essential for Treg and innate-like B cell development

Paracaspase activity controls NF-κB and mRNA stability regulators

Malt1 paracaspase activity prevents destructive autoinflammation

Authors

Andreas Gewies, Oliver Gorka, ..., Vigo Heissmeyer, Jürgen Ruland

Correspondence

jruland@lrz.tum.de

In Brief

The paracaspase Malt1 is a key regulator of antigen receptor signaling and frequently mutated in human lymphoma. Gewies et al. demonstrate that the proteolytic function of Malt1 is largely dispensable for lymphocyte activation but critical for regulatory T cell (Treg) and innate-like B cell development and protection from IFNγ-mediated autoinflammation in vivo.

Accession Numbers

GSE55360

Gewies et al., 2014, Cell Reports 9, 1292–1305
November 20, 2014 ©2014 The Authors
http://dx.doi.org/10.1016/j.celrep.2014.10.044

OPEN ACCESS
CellPress

Cell Reports
Article

Uncoupling Malt1 Threshold Function from Paracaspase Activity Results in Destructive Autoimmune Inflammation

Andreas Gewies,[1,2,16] Oliver Gorka,[1,16] Hanna Bergmann,[1] Konstanze Pechloff,[1,2] Franziska Petermann,[3] Katharina M. Jeltsch,[4,14] Martina Rudelius,[5] Mark Kriegsmann,[6] Wilko Weichert,[6] Marion Horsch,[7] Johannes Beckers,[7,8] Wolfgang Wurst,[9,10,11,12] Mathias Heikenwalder,[13] Thomas Korn,[3,10] Vigo Heissmeyer,[4,14] and Jürgen Ruland[1,2,15,*]

[1]Institut für Klinische Chemie und Pathobiochemie, Klinikum rechts der Isar, Technische Universität München, 81675 München, Germany
[2]German Cancer Consortium (DKTK) and German Cancer Research Center (DKFZ), 69120 Heidelberg, Germany
[3]Department of Neurology, Klinikum rechts der Isar, Technische Universität München, 81675 München, Germany
[4]Institute for Immunology, Ludwig-Maximilians-Universität München, Goethestraße 31, 80336 München, Germany
[5]Institute of Pathology, Julius-Maximilians-Universität Würzburg and Comprehensive Cancer Center Main-Franken, 97080 Würzburg, Germany
[6]Institut für Pathologie, Universitätsklinikum Heidelberg, 69120 Heidelberg, Germany
[7]Helmholtz Zentrum München – German Research Center for Environmental Health, Institute of Experimental Genetics, 85764 Neuherberg, Germany
[8]Institute of Experimental Genetics, Technische Universität München-Weihenstephan, 85350 Freising-Weihenstephan, Germany
[9]Helmholtz Zentrum München – German Research Center for Environmental Health, Institute of Developmental Genetics, 85764 Neuherberg, Germany
[10]Munich Cluster for Systems Neurology (SyNergy), 81675 München, Germany
[11]Technische Universität München-Weihenstephan, Institute of Developmental Genetics, c/o Helmholtz Zentrum München, 85764 Neuherberg, Germany
[12]Deutsches Zentrum für Neurodegenerative Erkrankungen e.V. (DZNE), Standort München, 80336 München, Germany
[13]Institute of Virology, Technische Universität München/Helmholtz Zentrum München, 81675 München, Germany
[14]Helmholtz Zentrum München, Institute of Molecular Immunology, 81377 München, Germany
[15]German Center for Infection Research (DZIF), partner site Munich, 81675 München, Germany
[16]Co-first author
*Correspondence: jruland@lrz.tum.de
http://dx.doi.org/10.1016/j.celrep.2014.10.044

SUMMARY

The paracaspase Malt1 is a central regulator of antigen receptor signaling that is frequently mutated in human lymphoma. As a scaffold, it assembles protein complexes for NF-κB activation, and its proteolytic domain cleaves negative NF-κB regulators for signal enforcement. Still, the physiological functions of Malt1-protease are unknown. We demonstrate that targeted Malt1-paracaspase inactivation induces a lethal inflammatory syndrome with lymphocyte-dependent neurodegeneration in vivo. Paracaspase activity is essential for regulatory T cell (Treg) and innate-like B cell development, but it is largely dispensable for overcoming Malt1-dependent thresholds for lymphocyte activation. In addition to NF-κB inhibitors, Malt1 cleaves an entire set of mRNA stability regulators, including Roquin-1, Roquin-2, and Regnase-1, and paracaspase inactivation results in excessive interferon gamma (IFNγ) production by effector lymphocytes that drive pathology. Together, our results reveal distinct threshold and modulatory functions of Malt1 that differentially control lymphocyte differentiation and activation pathways and demonstrate that selective paracaspase blockage skews systemic immunity toward destructive autoinflammation.

INTRODUCTION

Signals from antigen receptors (AgRs) control the development and activation of T and B lymphocytes during adaptive immunity. These pathways are essential for host defense against infections but can lead to immunodeficiency, autoimmunity, or cancer when dysregulated. The pathway that activates NF-κB transcription factors through the Card11, Bcl10, and Malt1 (CBM) protein complex is a key regulator of lymphocyte signaling for T and B cell differentiation and activation (Thome et al., 2010). Genetic deletion of any of these factors results in severe deficits in the development of regulatory T cells (Tregs), innate-like B1 B cells, and marginal zone B cells (Newton and Dixit, 2003; Ruefli-Brasse et al., 2003; Ruland et al., 2001, 2003). Moreover, although the differentiation of conventional T and B cells is largely intact in the absence of Card11/Bcl10/Malt1 signaling, all three factors are essential for productive lymphocyte activation. Consequently, loss-of-function mutations within the CBM complex result in severe combined immunodeficiencies in humans and

in mice (Greil et al., 2013; Jabara et al., 2013; McKinnon et al., 2014; Newton and Dixit, 2003; Ruefli-Brasse et al., 2003; Ruland et al., 2001, 2003). On the other hand, gain-of-function alterations of CBM signaling are recurrently detected in human non-Hodgkin lymphoma, where they trigger constitutive NF-κB activation, which is required for tumor cell survival (Staudt, 2010). These genomic aberrations include various independent chromosomal translocations involving Bcl10 or Malt1 and oncogenic mutations within Card11 in mucosa-associated lymphoid tissue (MALT) lymphoma and in diffuse large B cell lymphoma (Akagi et al., 1999; Lenz et al., 2008; Streubel et al., 2003; Willis et al., 1999).

Malt1 is the essential effector molecule within the CBM complex. This protein contains an amino-terminal death domain and immunoglobulin-like domains for protein-protein interactions and a proteolytically active paracaspase domain that shares homology with caspases and metacaspases. In resting lymphocytes, Malt1 is preassociated with Bcl10, and these two molecules coassociate with Card11 upon signal induction after T cell receptor (TCR) engagement or B cell receptor ligation (Thome et al., 2010). Malt1 acts as a scaffold, recruiting protein E3 ubiquitin ligases such as Traf6 to the newly formed CBM signalosome. This association leads to the nondegrading ubiquitination of Bcl10, Traf6, and Malt1 itself and thereby activates IκB kinase (IKK), which in turn promotes canonical NF-κB signaling by phosphorylating inhibitory IκB proteins, thereby inducing their degradation (Düwel et al., 2010). Malt1 further activates the JNK and p38 kinases (Ruland et al., 2003), which regulate transcription factors such as ATF2 (Gozdecka and Breitwieser, 2012). The proteolytic domain of Malt1, which has not been well defined at the physiological level, can cleave the A20 and CYLD deubiquitinases that target K63-type polyubiquitin chains, and it can negatively regulate NF-κB (Coornaert et al., 2008; Staal et al., 2011). In addition, Malt1 cleaves the NF-κB family member RelB, which also acts as an inhibitor of the canonical NF-κB pathway in T cells (Hailfinger et al., 2011). Moreover, Malt1 has recently been shown to cleave the endoribonuclease Regnase-1 (Uehata et al., 2013), which regulates the stability of mRNAs.

Because Malt1 has nonredundant activating roles in AgR signaling and possesses the only enzymatic activity within the CBM complex, extensive pharmaceutical efforts to develop Malt1 protease inhibitors for the treatment of prevalent chronic and malignant immune-mediated diseases are being pursued (Fontán and Melnick, 2013; Vucic and Dixit, 2009). Indeed, selective inhibition of MALT1 protease activity via peptide or small-molecule inhibitors is selectively toxic to human lymphoma cell lines that exhibit aberrant CBM activity (Ferch et al., 2009; Nagel et al., 2012). Moreover, because Malt1-deficient mice are protected from autoimmune diseases such as experimental autoimmune encephalomyelitis (Brüstle et al., 2012), it has been speculated that pharmaceutical agents that block Malt1 paracaspase activity could inhibit chronic inflammatory reactions in autoimmunity and would thus have the potential for use as anti-inflammatory immunosuppressors. Despite these endeavors, the physiological functions of Malt1 paracaspase activity and the differential roles of the Malt1 scaffold versus its proteolytic activity in lymphocyte development, activation, and immune homeostasis are unknown.

We report here that animals with a targeted Malt1 protease inactivation develop fatal inflammation with neurodegeneration. Although the paracaspase activity of Malt1 is largely dispensable for overcoming the Malt1-controlled threshold for lymphocyte activation, this activity is essential for the differentiation of lymphocytes including Tregs, marginal zone B cells, and B1 B cells. In activated conventional T cells, Malt1 cleaves, in parallel with NF-κB inhibitors, an entire set of mRNA stability factors that includes Roquin-1 and Roquin-2 in addition to Regnase-1. Also, Malt1 proteolytic inactivation results in excessive interferon gamma (IFNγ) production that mediates inflammatory pathology. Our data demonstrate differential regulation of lymphocyte differentiation and activation pathways by Malt1 and reveal that Malt1 protease inhibition results in spontaneous lethal autoinflammation.

RESULTS

Systemic Inflammation in the Absence of Malt1 Paracaspase Activity

To selectively inactivate Malt1 enzymatic activity in vivo, we replaced the active site cysteine within its protease domain with alanine (C472A; Figures S1A and S1B). Mice with one or two *Malt1* *p*aracaspase *m*utant (*Malt1*^{PM}) alleles were viable and born in Mendelian ratios similarly to *Malt1*-deficient (*Malt1*$^{-/-}$) animals (data not shown). Western blotting of splenic lysates demonstrated that paracaspase mutant Malt1 protein expression in *Malt1*$^{PM/-}$ mice was comparable to Malt1 wild-type protein expression in *Malt1*$^{+/-}$ mice (Figure 1A). To assay catalytic activity, we stimulated splenocytes with phorbol 12-myristate 13-acetate and ionomycin (PMA/Iono). Signal-induced cleavage of the Malt1 substrate Ac-LRSR-AMC (Nagel et al., 2012) was detected in activated splenocytes from Malt1$^{+/-}$ mice, but not in those from Malt1$^{-/-}$ or in Malt1$^{PM/-}$ animals (Figure 1B). Thus, although the paracaspase mutant Malt1 protein was expressed normally, it did not have proteolytic function.

Although Malt1$^{-/-}$ mice are immunodeficient, the absence of Malt1 does not affect animal growth or viability under homeostatic conditions, and *Malt1*$^{-/-}$ mice reach a normal age without overt pathology (Ruefli-Brasse et al., 2003; Ruland et al., 2003). In sharp contrast, the Malt1$^{PM/-}$ paracaspase mutant mice failed to thrive and started to develop severe cachexia (Figure 1C) and lymphadenopathy with a strong increase in the numbers of T and B cells (Figure 1D). *Malt1*$^{PM/-}$ mice developed a systemic inflammatory disorder characterized by highly elevated serum concentrations of the inflammatory cytokines IFNγ and tumor necrosis factor (TNF) already at an age of 6 to 10 weeks (Figure 1E), whereas serum cytokine levels of interleukin 1β (IL-1β), IL-17, and IL-6 were not substantially elevated in *Malt1*$^{PM/-}$ mice (Figure S2A). Of note, also *Malt1*$^{PM/PM}$ homozygous paracaspase-deficient mice developed the same disease phenotype as observed for *Malt1*$^{PM/-}$ mice (Figures S2B and S2D; data not shown). Importantly, *Malt1*$^{PM/+}$ animals, which carry only one mutated allele but additionally express the proteolytic active Malt1 form, did not exhibit these pathologies (Figures S2B–S2D and data not shown), indicating that the mutant protein does not behave as a dominant-negative factor.

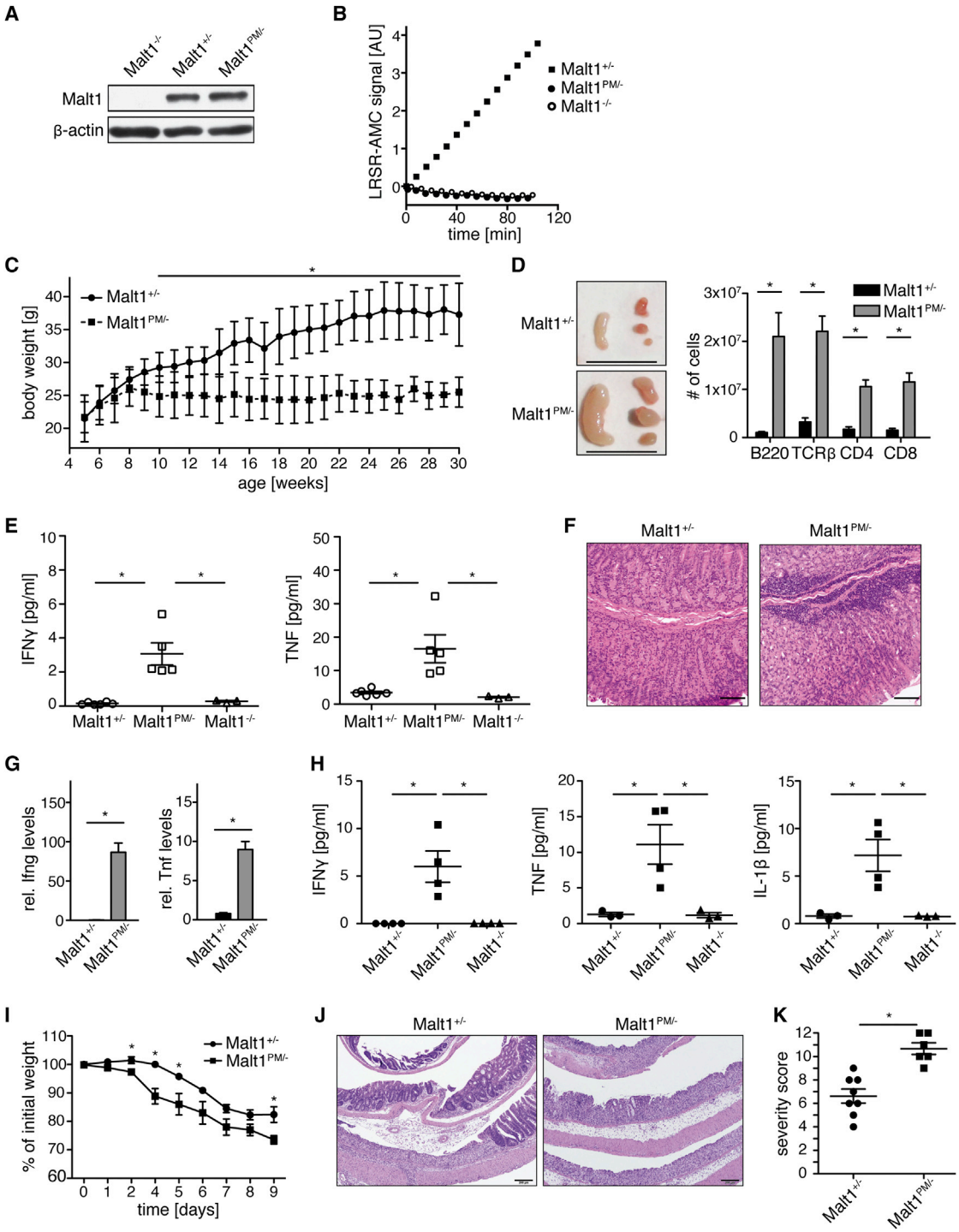

Figure 1. Malt1 Protease Inactivation Results in Systemic Inflammation and Dysregulated Mucosal Immune Homeostasis

(A) Immunoblot of protein extracts from *Malt1*$^{+/-}$, *Malt1*$^{-/-}$, and *Malt1*$^{PM/-}$ splenocytes for the detection of Malt1 and β-actin expression.

(B) LRSR-AMC cleavage assay with stimulated T cells from *Malt1*$^{+/-}$, *Malt1*$^{-/-}$, and *Malt1*$^{PM/-}$ mice. The results are representative of three independent experiments.

(C) Body weight curves for *Malt1*$^{+/-}$ and *Malt1*$^{PM/-}$ mice (n > 6 per time point, two-tailed unpaired t test).

(D) Photos displaying representative mesenteric (left) and cervical (right) lymph nodes from *Malt1*$^{+/-}$ mice and *Malt1*$^{PM/-}$ mice at 8 weeks of age (scale bar, 1 cm). The bar graph shows total numbers of B and T cells in the cervical lymph nodes from *Malt1*$^{+/-}$ and *Malt1*$^{PM/-}$ mice at 8 to 10 weeks of age (right panel, mean ± SEM, n = 4 each, two-tailed unpaired t test).

(legend continued on next page)

We focused the further analysis on a comparison of the *Malt1*$^{PM/-}$ mice with *Malt1*$^{+/-}$ and *Malt1*$^{-/-}$ mice. Histological analysis of the Malt1$^{PM/-}$ animals showed T and B cell organ infiltration. Mixed lymphocytic infiltrates were detected in the gastric mucosa of *Malt1*$^{PM/-}$ mice (Figure 1F) with locally increased inflammatory cytokine expression (Figure 1G). In vitro colon cultures also showed spontaneous production of high IFNγ, TNF, and IL-1β levels in *Malt1*$^{PM/-}$, but not *Malt1*$^{-/-}$ or *Malt*$^{+/-}$, samples (Figure 1H). In a model of inflammatory bowel disease, we treated the animals with 3.5% dextran sodium sulfate (DSS) for 5 days to trigger intestinal epithelial damage (Oh et al., 2014). Malt1$^{PM/-}$ mice developed a more rapid and aggravated inflammatory disease compared to control mice, with severe hemorrhagic diarrhea, increased weight loss (Figure 1I), and an elevated histological severity score (Figures 1J and 1K).

Starting from 3 months of age, all *Malt1*$^{PM/-}$ mutant mice suffered from a spontaneous neurological disorder with dystonia and progressive ataxia (Figures 2A and 2B), indicative of a cerebellar defect. Rotarod analysis was used to quantitatively characterize this motor-coordination deficit (Shiotsuki et al., 2010). Whereas *Malt1*$^{+/-}$ and *Malt1*$^{-/-}$ mice stayed on the rotating rod for a minimum of 120 s, the *Malt1*$^{PM/-}$ animals failed to accomplish this task even after numerous trials (Figure 2C; see also Figure 2H). Loss of Purkinje cells is associated with severe ataxic syndromes (Kullmann et al., 2012). Histopathological analysis of the CNS indeed showed a marked reduction of Purkinje cells in the cerebellar cortex of *Malt1*$^{PM/-}$ mice (Figure 2D). Notably, we also observed elevated numbers of CD4$^+$ and CD8$^+$ T lymphocytes in the brains of *Malt1*$^{PM/-}$ mice compared to control animals (Figure 2E). To determine the role of lymphocytes in the systemic inflammation and neurodegeneration, we crossed *Malt1*$^{PM/-}$ mice to *Rag1*-deficient animals, which lack T and B cells. Moreover, we wanted to test whether disease in the paracaspase mutants is caused by aberrant Malt1 signaling from within canonical Bcl10/Malt1 complexes or whether the catalytically inactive Malt1 protein mediates its pathological effects via Bcl10-independent mechanisms. Thus, we also crossed the *Malt1*^{PM} allele into a *Bcl10*-deficient background. The absence of Bcl10 prevented both systemic inflammation and ataxia (Figures 2F and 2G), and the lack of lymphocytes in the *Rag1*$^{-/-}$ background also completely rescued *Malt1*$^{PM/-}$ mice from disease, normalized the levels of inflammatory cytokines in the blood (Figure 2F), and prevented the development of neurological defects as determined by clinical ataxia scoring (Figure 2G) and rotarod analysis (Figure 2H). Altogether, these in vivo observations reveal a counterintuitive autoinflammatory condition and neuropathology upon selective Malt1 paracaspase inactivation. Moreover, the results indicate that these disorders are caused by aberrant Malt1 function within Bcl10-containing complexes, and they prove genetically that the pathology in Malt1 paracaspase mutant mice is dependent on aberrant lymphocyte activity.

Differential Control of Lymphocyte Differentiation and Activation Signals

Because of the findings above, we next studied lymphocyte differentiation and activation in *Malt1*$^{PM/-}$ mice prior to the onset of cachexia. Flow cytometric analysis of T cell differentiation in the thymi of *Malt1*$^{PM/-}$ mice revealed normal numbers and frequencies of double-negative, double-positive, and CD4 or CD8 single-positive T cells similar to those in *Malt1*-deficient mice (Ruefli-Brasse et al., 2003; Ruland et al., 2003), indicating normal thymic T cell differentiation (Figure 3A). However, *Malt1*$^{PM/-}$ mice almost completely lacked CD4$^+$CD25$^+$Foxp3$^+$ thymic regulatory T cells, similarly to *Malt1*$^{-/-}$ mice (Figure 3B).

Early B cell development in the bone marrow was not affected in *Malt1*$^{PM/-}$ mice, as these animals exhibited normal distributions of pre/pro B cells (B220^{low}IgM$^-$), immature B cells (B220^{low}IgM$^+$), and recirculating B cells (B220^{high}IgM$^+$) (Figure 3C). Neither the total number of peripheral B cells nor the frequencies of immature (B220$^+$IgM$^+$IgD$^-$) or mature (B220$^+$IgM$^-$IgD$^+$) B2 B cells differed among the *Malt1*$^{+/-}$, *Malt1*$^{PM/-}$, and *Malt1*$^{-/-}$ mice (data not shown). However, the B220$^+$CD21^{high}CD23^{low} splenic marginal B cell population was almost completely absent in *Malt1*$^{PM/-}$ mice (Figure 3D), and the frequency of peritoneal B1 B cells (CD19$^+$B220^{low}) (Figure 3E) was also severely reduced in *Malt1*$^{PM/-}$ mice, similar to the results observed in *Malt1*-deficient mice (Ruefli-Brasse et al., 2003; Ruland et al., 2003). Thus, the Malt1-dependent signals for Treg development and innate-like marginal zone and B1 B cell generation are strictly dependent on Malt1 proteolytic activity.

We further detected significant increases in the percentages of CD8$^+$ memory T cells (CD62L$^+$CD44$^+$) and CD4$^+$ and CD8$^+$ effector memory T cells (CD62L$^-$CD44$^+$) in the spleens of *Malt1*$^{PM/-}$ animals when compared to those from either *Malt1*$^{+/-}$ or *Malt1*$^{-/-}$ mice, whereas the pool of naive T cells was reduced in *Malt1*$^{PM/-}$ animals (Figure 4A). Because memory and effector memory cells arise from naive T cells after activation, these data suggest that a substantial proportion of conventional *Malt1*$^{PM/-}$ T cells might have received a productive TCR signal in vivo. To directly test the paracaspase function in T cell activation, we

(E) Serum concentrations of IFNγ and TNF were measured for *Malt1*$^{+/-}$ (n = 6), *Malt1*$^{-/-}$ (n = 3), and *Malt1*$^{PM/-}$ (n = 5) mice at 6 to 8 weeks of age. Horizontal bars indicate the mean ± SEM (two-tailed unpaired t test).

(F) Representative histologies of hematoxylin and eosin (H&E)-stained stomachs from *Malt1*$^{+/-}$ and *Malt1*$^{PM/-}$ littermates at 16 weeks demonstrating lymphocyte infiltration in *Malt1*$^{PM/-}$ mice. Scale bars indicate 100 μm.

(G) Real-time PCR analysis of reverse-transcribed RNA obtained from stomach tissue samples of *Malt1*$^{+/-}$ and *Malt1*$^{PM/-}$ mice at 16 weeks. Bars indicate the relative IFNγ and TNF transcript levels (mean ± SEM, n = 4 each, two-tailed unpaired t test).

(H) Colon tissue samples from untreated *Malt1*$^{+/-}$, *Malt1*$^{PM/-}$, and *Malt1*$^{-/-}$ mice at an age of 12 weeks were cultured for 48 hr, and cytokine concentrations of IFNγ, TNF, and IL-1β were measured by cytometric bead array. Horizontal bars indicate the mean ± SEM (n = 3–4, two-tailed unpaired t test).

(I) Body weight curves of *Malt1*$^{+/-}$, *Malt1*$^{PM/-}$, and *Malt1*$^{-/-}$ mice during DSS treatment. The data show the percentages of initial weight prior to treatment (mean ± SEM; starting with six to eight animals per group, two-tailed unpaired t test).

(J) Representative H&E-stained colon tissue sections from *Malt1*$^{+/-}$ and *Malt1*$^{PM/-}$ mice after DSS treatment. Scale bars indicate 200 μm.

(K) Severity score of DSS-induced colitis in *Malt1*$^{+/-}$ (n = 8) and *Malt1*$^{PM/-}$ mice (n = 6) by evaluation of colon histology. Horizontal bars indicate the mean ± SEM, Mann-Whitney test. *$p < 0.05$.

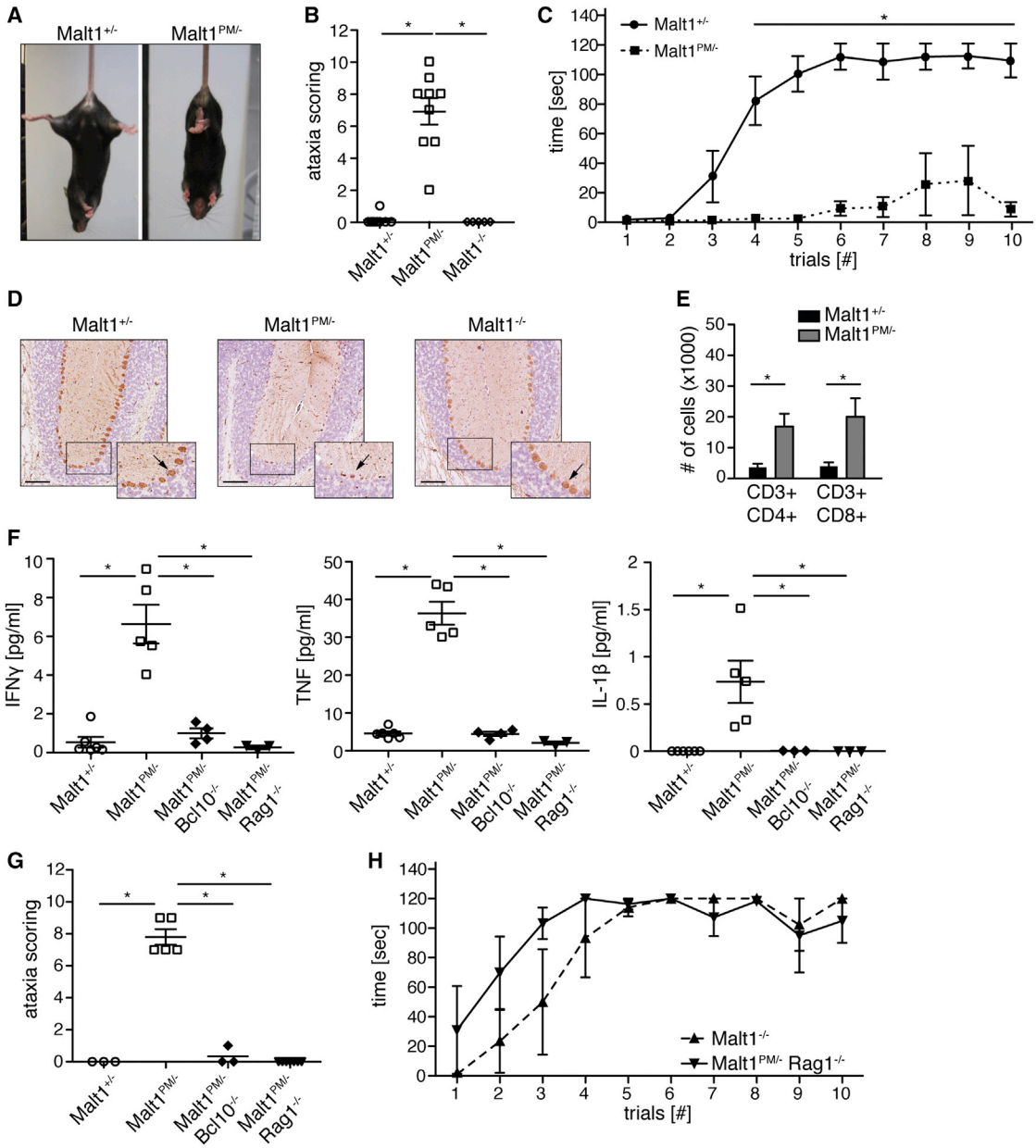

Figure 2. Lymphocyte-Dependent Systemic Inflammation and Neurodegeneration in Paracaspase Mutant Mice

(A) Hindlimb clasping as observed for a representative *Malt1*$^{PM/-}$ mouse compared to a *Malt1*$^{+/-}$ control.

(B) Ataxia severity scores for *Malt1*$^{+/-}$ (n = 10), *Malt1*$^{PM/-}$ (n = 10), and *Malt1*$^{-/-}$ mice (n = 5) at an age between 3 and 6 months. Horizontal bars indicate the mean ± SEM, Mann-Whitney test.

(C) The motor coordination of *Malt1*$^{+/-}$ and *Malt1*$^{PM/-}$ mice was tested in a rotarod experiment with ten consecutive trials at 4 to 5 months of age. The data show the mean duration of the trials (mean ± SEM; n = 4 each, two-tailed unpaired t test).

(D) Cerebellar section from representative atactic *Malt1*$^{PM/-}$ mice and age-matched (>20 weeks) *Malt1*$^{+/-}$ and *Malt1*$^{-/-}$ control animals were stained with anti-calbindin in order to visualize Purkinje cells (arrow). Scale bars indicate 100 μm.

(E) Absolute numbers of CD4$^+$ and CD8$^+$ T lymphocytes in the brains of *Malt1*$^{+/-}$ and *Malt1*$^{PM/-}$ mice at an age of 4–5 months were determined by flow cytometry (mean ± SEM; n = 3 each, two-tailed unpaired t test).

(F) IFNγ, TNF, and IL-1β levels in the serum of *Malt1*$^{+/-}$, *Malt1*$^{PM/-}$, *Malt1*$^{PM/-}$;*Bcl10*$^{-/-}$, and *Malt1*$^{PM/-}$;*Rag1*$^{-/-}$ mice at 3–4 months of age. Horizontal bars indicate the mean ± SEM (n = 3–6, two-tailed unpaired t test).

(G) Ataxia scoring of *Malt1*$^{+/-}$ (n = 3), *Malt1*$^{PM/-}$ (n = 5), *Malt1*$^{PM/-}$;Bcl10$^{-/-}$ (n = 3), and *Malt1*$^{PM/-}$;*Rag1*$^{-/-}$ mice (n = 7) at an age between 7 and 9 months. Horizontal bars indicate the mean ± SEM, Mann-Whitney test.

(H) The motor coordination of composite *Malt1*$^{PM/-}$, *Rag1*$^{-/-}$ (n = 4), and *Malt1*$^{-/-}$ mice (n = 3) was tested at an age of 4–5 months in the same set of rotarod experiments as shown in (C). The data show the mean duration of the trials (mean ± SEM).

*$p < 0.05$.

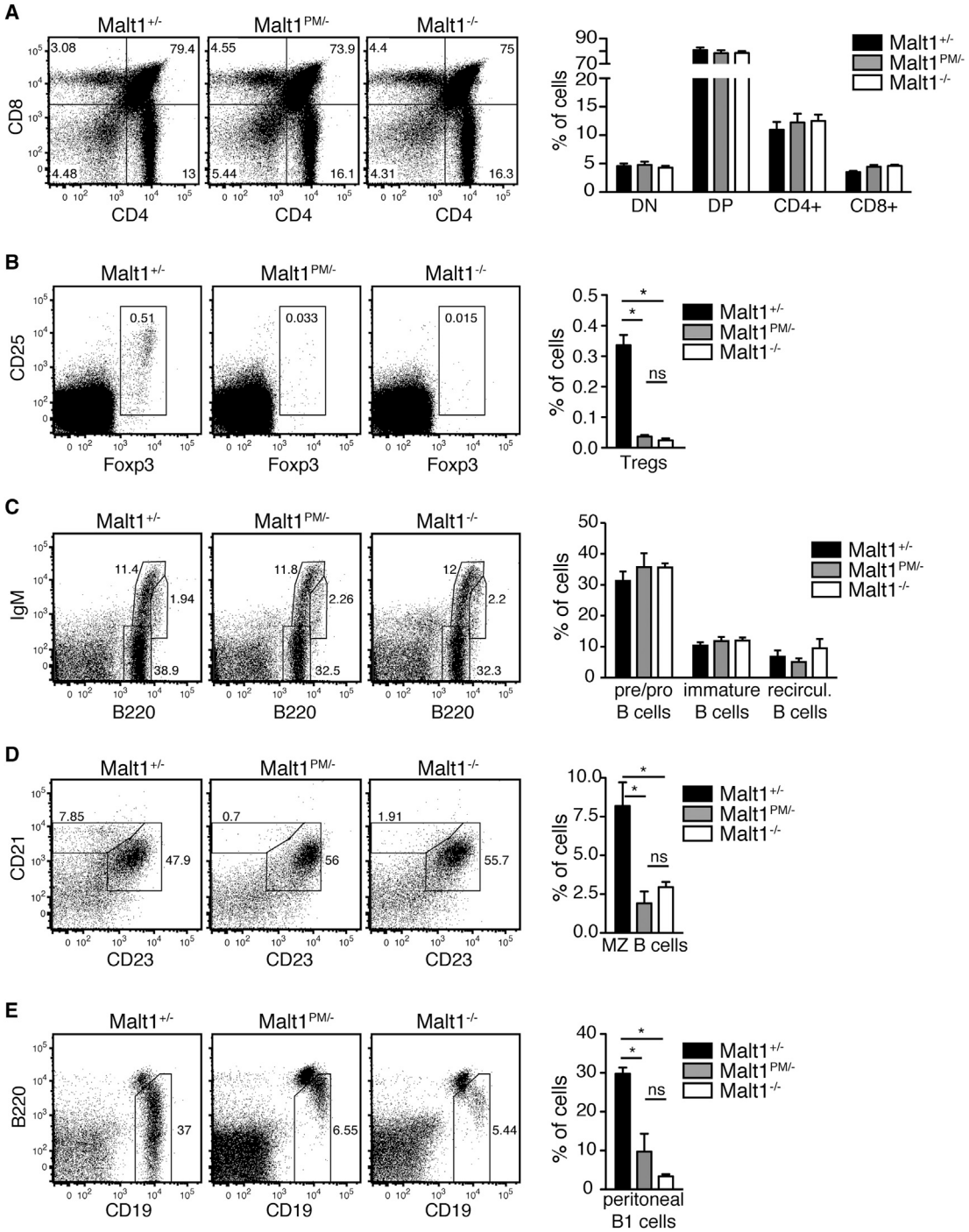

Figure 3. Paracaspase Activity Controls Treg and Innate B Cell Development

(A) Flow cytometry of thymic T cell populations of *Malt1*$^{+/-}$ (n = 10), *Malt1*$^{PM/-}$ (n = 8), and *Malt1*$^{-/-}$ mice (n = 6) characterized by surface CD4 and CD8 staining.

(B) Thymus-derived regulatory T cells of *Malt1*$^{+/-}$ (n = 10), *Malt1*$^{PM/-}$ (n = 8), and *Malt1*$^{-/-}$ mice (n = 6) were measured by flow cytometry after extracellular CD4 and CD25 staining and intracellular Foxp3 staining.

(C) Flow cytometry of pre/pro-B cells (B220 low, IgM−), immature B cells (B220 low, IgM+), and recirculating B cells (B220 high, IgM+) in the bone marrow of *Malt1*$^{+/-}$ (n = 9), *Malt1*$^{PM/-}$ (n = 7), and *Malt1*$^{-/-}$ mice (n = 5).

(D) Flow cytometry of marginal zone B cells (CD21^{+}CD23^{-}) in spleens of *Malt1*$^{+/-}$, *Malt1*$^{PM/-}$, and *Malt1*$^{-/-}$ mice (n = 4 each).

(E) Flow cytometry of peritoneal B1 cells (CD19^{+}B220^{lo}) in *Malt1*$^{+/-}$ (n = 6), *Malt1*$^{PM/-}$ (n = 5), and *Malt1*$^{-/-}$ mice (n = 5). The dot plot graphs display representative flow cytometry results, and bar graphs show the mean ± SEM (two-tailed unpaired t test).

All analyses were performed with animals at 8 to 10 weeks of age. *$p < 0.05$; ns, not significant.

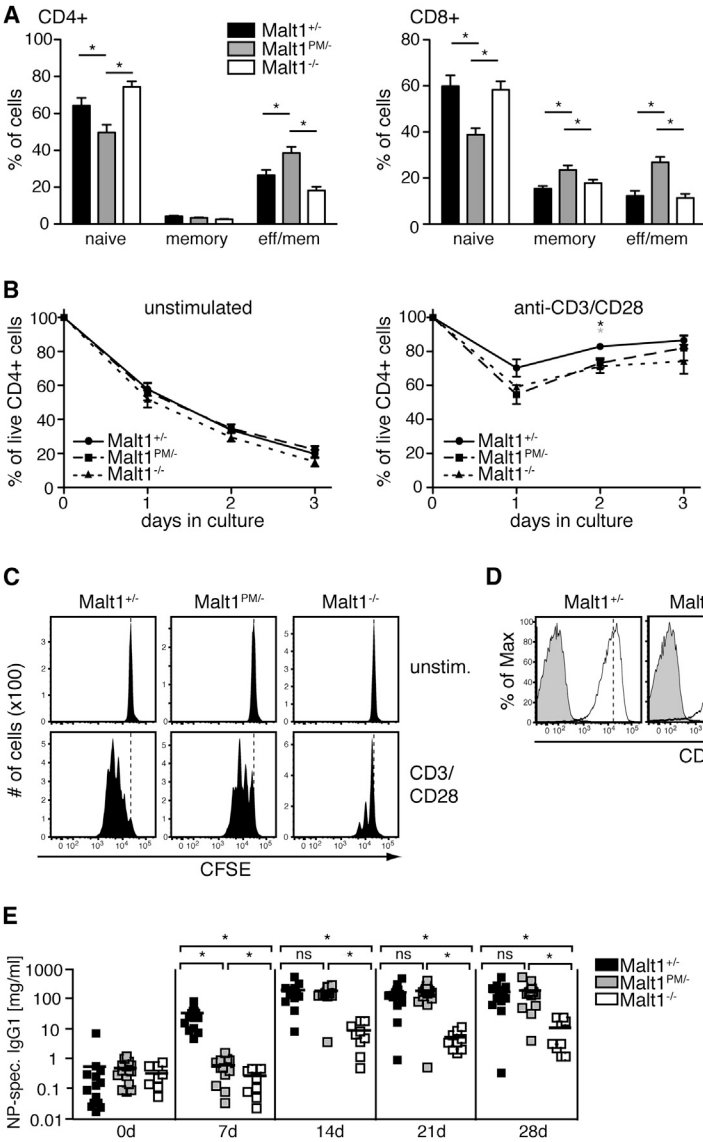

Figure 4. Paracaspase Activity Is Largely Dispensable for Malt1-Mediated Lymphocyte Activation

(A) Flow cytometry of naive ($CD62L^+CD44^-$), memory ($CD62L^+CD44^+$), and effector/memory T cells ($CD62L^-CD44^+$) in spleens of *Malt1*$^{+/-}$ (n = 11), *Malt1*$^{PM/-}$ (n = 9), and *Malt1*$^{-/-}$ mice (n = 6) within the $CD4^+$ (left) and $CD8^+$ (right) subsets. The bar graphs show the mean ± SEM (two-tailed unpaired t test).

(B) Viability of purified $CD4^+$ T cells from *Malt1*$^{+/-}$, *Malt1*$^{-/-}$, and *Malt1*$^{PM/-}$ mice (n = 4 each) cultured in vitro either unstimulated (left) or stimulated with anti-CD3/CD28 (right). At the indicated time points, the percentage of living cells was determined by Annexin V/7-AAD staining in flow cytometry (mean ± SEM, two-tailed unpaired t test).

(C) Cell division of isolated $CD4^+$ T cells from *Malt1*$^{+/-}$, *Malt1*$^{PM/-}$, and *Malt1*$^{-/-}$ mice investigated by carboxyfluorescein succinimidyl ester (CFSE) flow cytometry after stimulation with plate-bound anti-CD3/CD28 for 72 hr. The data are representative of three experiments.

(D) Flow cytometry of CD25 activation marker expression in naive T cells of the respective genotypes after 18 hr of stimulation with anti-CD3/CD28. Red lines indicate median values in the *Malt1*$^{+/-}$ T cells after stimulation. The data are representative of three experiments.

(E) IgG1 immunoglobulin levels in the sera of *Malt1*$^{+/-}$ (n = 18), *Malt1*$^{PM/-}$ (n = 15), and *Malt1*$^{-/-}$ mice (n = 9) after NP-OVA immunization measured by NP-specific ELISA. Sera were collected at the indicated time points after immunization. The data are shown in a logarithmic scale with horizontal bars indicating the means (two-tailed unpaired t test).

All analyses were performed with animals at 8 to 10 weeks of age. *p < 0.05; ns, not significant.

purified naive T lymphocytes from *Malt1*$^{+/-}$, *Malt1*$^{PM/-}$, and *Malt1*$^{-/-}$ animals and stimulated these via their AgR in vitro. Compared to the wild-type, both *Malt1*$^{PM/-}$ and *Malt1*$^{-/-}$ $CD4^+$ T cells showed slightly reduced viability after 2 days of stimulation in vitro (Figure 4B). However, whereas the surviving *Malt1*$^{-/-}$ T cells exhibited severely impaired TCR-induced proliferation as expected (Ruefli-Brasse et al., 2003; Ruland et al., 2003), *Malt1*$^{PM/-}$ T cells divided vigorously, although their proliferation rate was suboptimal when compared to *Malt1*$^{+/-}$ T cells (Figure 4C). Moreover, in contrast to the complete Malt1 deletion, paracaspase inactivation failed to affect the upregulation of the activation marker CD25 (Figure 4D).

Next, we immunized the animals with (4-hydroxy-3-nitrophenyl)acetyl-ovalbumin (NP-OVA) to study antigen-specific lymphocyte activation in vivo. Again, as expected, the T cell-dependent production of NP-specific immunoglobulin G1 (IgG1) antibodies was defective in *Malt1*$^{-/-}$ mice (Figure 4E) (Ruefli-Brasse et al., 2003; Ruland et al., 2003). However, *Malt1*$^{PM/-}$ mice produced normal amounts of antigen-specific IgG1 2 weeks after immunization, although their adaptive immune response was delayed (Figure 4E). Together, these data demonstrate that the paracaspase activity of Malt1 is, to a considerable extent, dispensable for Malt1-controlled lymphocyte activation pathways in vitro and in vivo.

Threshold and Modulatory Activity of Malt1 in TCR Signaling

We next isolated naive $CD4^+$ T cells for biochemical analysis. As previously shown, Malt1 ablation blocks PMA/Iono-induced and anti-CD3/anti-CD28-induced IKK activation (Figures 5A and 5D), and the MAP kinases p38 and Jnk were also not activated in Malt1$^{-/-}$ T cells despite normal Erk signaling (Figure 5B) (Ruefli-Brasse et al., 2003; Ruland et al., 2003). In contrast, the selective paracaspase mutation did not impair IKK, p38, or Jnk activation (Figures 5A and 5B). Consistently, IκBα was phosphorylated and degraded normally (Figures 5A and 5D), and

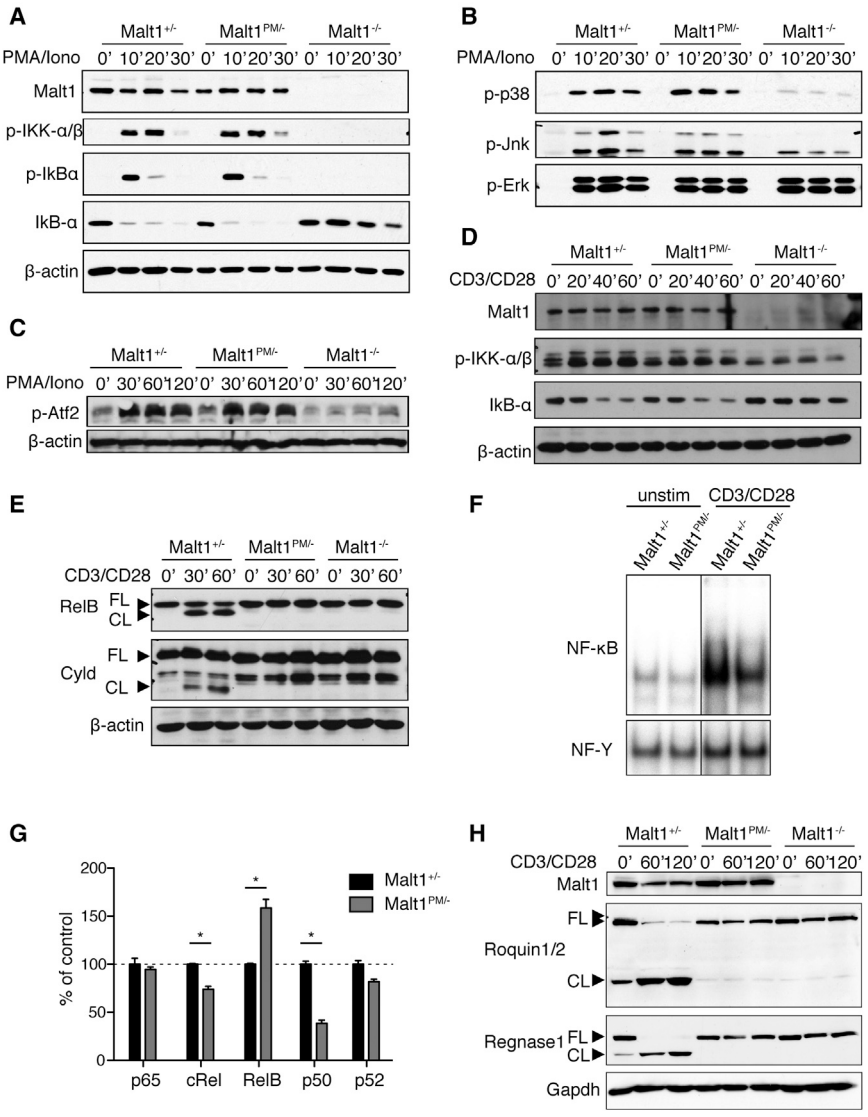

Figure 5. Threshold and Modulatory Activity of Malt1 in TCR Signaling

(A) Purified naive CD4$^+$ T cells from *Malt1*$^{+/-}$, *Malt1*$^{-/-}$, and *Malt1*$^{PM/-}$ mice were stimulated for the indicated time points with PMA and ionomycin and analyzed by western blot with antibodies against Malt1, phospho-IKKα/β, phospho-IκBα, IκBα, and β-actin as a loading control. The results are representative of three independent experiments.

(B) To test MAP kinase signaling, the same extracts as used in (A) were analyzed by immunoblot using antibodies to phospho-p38, phospho-Jnk, and phospho-Erk.

(C) CD4$^+$ T cells from *Malt1*$^{+/-}$, *Malt1*$^{PM/-}$, and *Malt1*$^{-/-}$ mice were stimulated with PMA and ionomycin for the indicated time points. Cell lysates were analyzed by western blot with antibodies against phospho-Atf-2 and anti-β-actin.

(D) Purified CD4$^+$ T cells from *Malt1*$^{+/-}$, *Malt1*$^{-/-}$, and *Malt1*$^{PM/-}$ mice were stimulated for the indicated time points with plate-bound anti-CD3 (5 μg/ml) and soluble anti-CD28 (2 μg/ml) in the presence of cycloheximide (10 μg/ml) and analyzed by western blot with antibodies against Malt1, phospho-IKKα/β, IκBα, and β-actin.

(E) CD4$^+$ T cells from *Malt1*$^{+/-}$, *Malt1*$^{PM/-}$, and *Malt1*$^{-/-}$ mice were stimulated with plate-bound anti-CD3 (5 μg/ml) and soluble anti-CD28 (2 μg/ml) for the indicated time points in the presence of the proteasome inhibitor MG132 (10 μg/ml). Cell lysates were analyzed by immunoblot using antibodies specific for RelB, Cyld, and β-actin.

(F) CD4$^+$ T cells were left unstimulated or were stimulated for 8 hr by plate-bound anti-CD3 and anti-CD28. The DNA binding activity of the nuclear extracts was analyzed by an electrophoretic mobility shift assay using oligos with NF-κB binding sites or NF-Y binding sites as a control.

(G) Naive CD4$^+$ T cells were treated as in (F). Nuclear extracts were prepared and DNA binding activities of specific NF-κB subunits were quantified by an ELISA-based assay. For each subunit, the data from three experiments were normalized to *Malt1*$^{+/-}$ control T cells and are expressed as the mean ± SEM (two-tailed unpaired t test).

(H) CD4$^+$ T cells from *Malt1*$^{+/-}$, *Malt1*$^{PM/-}$, and *Malt1*$^{-/-}$ mice were stimulated as in (E). Cell lysates were analyzed by immunoblot using antibodies specific for Malt1, Roquin1/2, Regnase1, and Gapdh.

All analyses were performed with animals at 8 to 10 weeks of age. *$p < 0.05$.

the transcription factor Atf2 was also phosphorylated normally in *Malt1*$^{PM/-}$ T cells, but not in *Malt1*-deficient T cells (Figure 5C).

Next, we investigated the cleavage of candidate Malt1 substrates in primary *Malt1*$^{PM/-}$ T cells stimulated with anti-CD3/anti-CD28 or with PMA/Iono. Robust signal-induced proteolysis of RelB and Cyld was observed in T cells from *Malt1*$^{+/-}$ mice, but not in T cells from *Malt1*$^{-/-}$ or *Malt1*$^{PM/-}$ mice (Figures 5E and S3A). Due to the lack of an antibody that recognizes cleaved murine A20, we were unable to study endogenous A20 processing. Because these Malt1 targets can negatively regulate canonical NF-κB activity (Hailfinger et al., 2011; Reiley et al., 2007), we measured NF-κB DNA binding 8 hr after T cell stimulation. Electromobility shift assays revealed suboptimal NF-κB DNA binding in *Malt1*$^{PM/-}$ T cells (Figure 5F). In line with the defective cleavage of RelB (Figure 5E), stimulated T cells from *Malt1*$^{PM/-}$ mice showed increased amounts of nuclear RelB DNA-binding compared to *Malt1*$^{+/-}$ T cells (Figure 5G). Moreover, the DNA-binding activities of c-Rel and p50 were significantly reduced in *Malt1*$^{PM/-}$ mice, whereas p65 DNA binding was not affected by mutation of the paracaspase (Figure 5G). Thus, the paracaspase activity of Malt1 fine-tunes canonical NF-κB activity after initial IKK activation and particularly controls the full nuclear DNA binding of the NF-κB subunits p50 and c-Rel.

Immune-modulatory gene expression is not only controlled by transcription factors but also strongly regulated at the level of mRNA stability (Cheadle et al., 2005; Vogel et al., 2013).

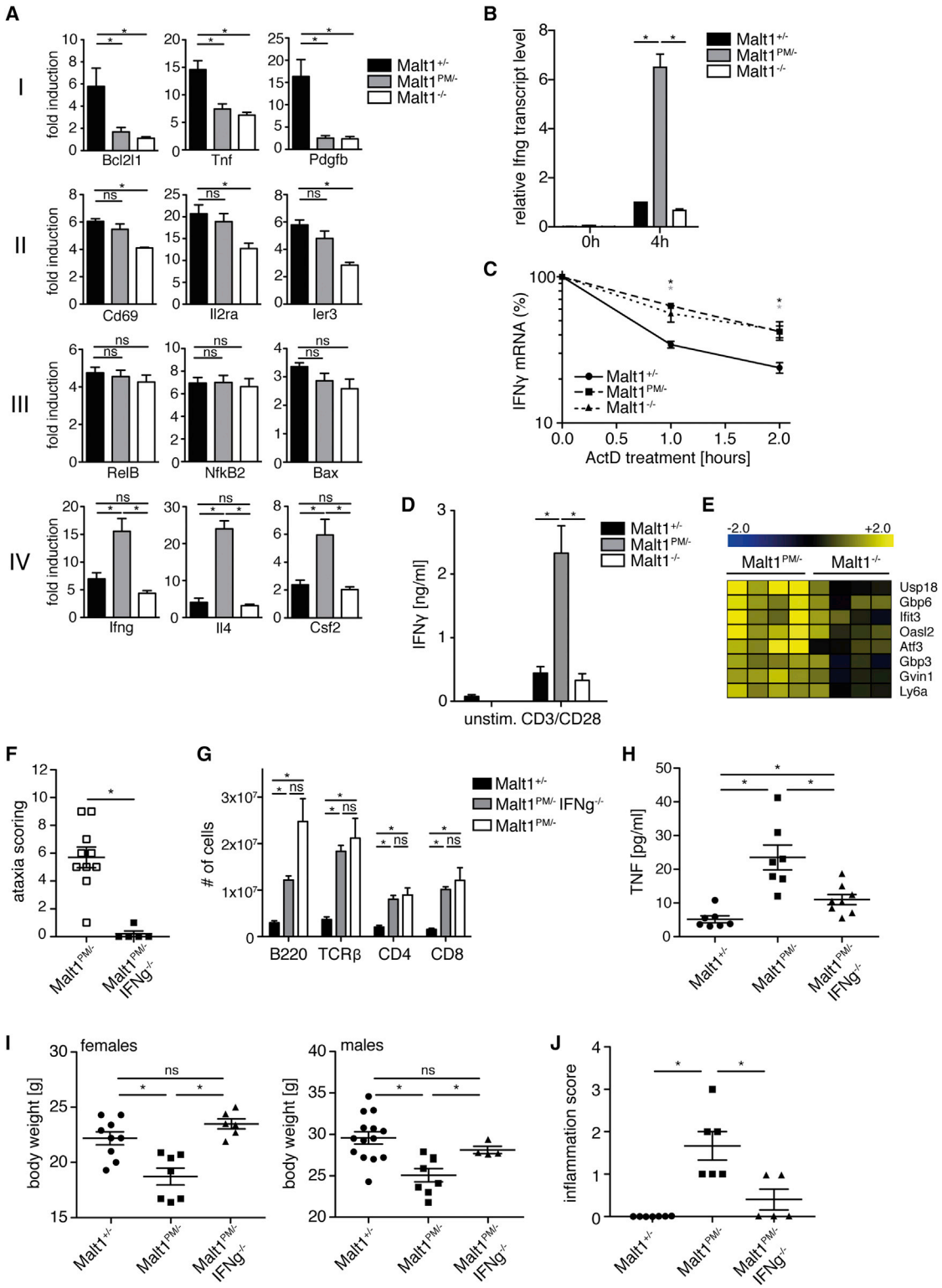

Figure 6. mRNA Expression and IFNγ Production in Malt1 Mutant T Cells

(A) FACS-sorted naive CD4$^+$CD62L$^+$CD25$^-$ T cells from *Malt1*$^{+/-}$, *Malt1*$^{PM/-}$, and *Malt1*$^{-/-}$ mice (n = 4 each) were left unstimulated or were stimulated for 4 hr with anti-CD3 and anti-CD28. Total RNA was isolated, and gene expression profiling was performed. The microarray data were analyzed for the expression of NF-κB target genes that were >2-fold upregulated upon TCR stimulation in at least one of the three genotypes. The upregulated genes could be classified into four

(legend continued on next page)

Regnase-1 was recently identified as a Malt1 substrate that controls mRNA stability (Uehata et al., 2013), and we discovered independently that Malt1 can cleave the RNA-binding proteins Roquin-1 and Roquin-2 (Jeltsch et al., 2014). Similar to Regnase-1, the Roquin paralogs bind to stem-loop structures in the 3′ UTRs of target mRNAs to control their decay (Leppek et al., 2013). To define the requirement for Malt1 proteolysis of Regnase-1 and Roquin degradation, we performed western blots using either an anti-Regnase-1 antibody or a monoclonal antibody that recognizes a conserved N-terminal epitope in Roquin-1 and Roquin-2 using lysates from activated T cells. The Roquin proteins were completely degraded in stimulated wild-type T cells, and the proteolysis of the Roquins was strictly dependent on Malt1 proteolytic activity (Figures 5H and S3B). Moreover, Regnase-1 cleavage was observed in wild-type T cells but was abolished in *Malt1*$^{PM/-}$ T cells, similar to the results in *Malt1*$^{-/-}$ T cells (Figures 5H and S3C).

Malt1 Protease Activity Prevents Pathological Overproduction of IFNγ

The simultaneous functions of Malt1-mediated proteolysis in signal-dependent NF-κB control and the cleavage of mRNA decay factors prompted us to investigate the overall impact of the paracaspase mutation on TCR-induced mRNA expression. To this end, we fluorescence-activated cell sorting (FACS)-purified naive (CD4$^+$CD62L$^+$CD25$^-$) T cells from *Malt1*$^{+/-}$, *Malt1*$^{PM/-}$, and *Malt1*$^{-/-}$ mice, stimulated these cells via the TCR, and performed microarray mRNA expression analysis. First, we focused on NF-κB target mRNAs (as defined in the Supplemental Experimental Procedures) that were at least 2-fold upregulated in at least one of the three genotypes. Statistical criteria subdivided these mRNAs into qualitatively distinct groups (Figure 6A). The first group includes mRNAs such as the c-Rel target Bcl2l1 that were robustly upregulated in Malt1$^{+/-}$ cells and not upregulated or significantly less so in *Malt1*$^{PM/-}$ and *Malt1*$^{-/-}$ T cells. The second includes NF-κB targets such as IL-2 receptor-alpha (CD25) that were comparably upregulated in *Malt1*$^{+/-}$ and *Malt1*$^{PM/-}$ T cells but significantly less so in *Malt1*$^{-/-}$ T cells. The third group includes mRNAs such as NF-κB2 that were upregulated similarly in all three genotypes. The findings are in principle in line with differential control of the NF-κB response via Malt1's scaffold and protease functions.

Surprisingly, we also identified a fourth group of NF-κB-regulated genes, including the inflammatory cytokine IFNγ, that show much higher mRNA expression in stimulated *Malt1*$^{PM/-}$ T cells compared to either *Malt1*$^{+/-}$ or *Malt1*$^{-/-}$ T cells (Figure 6A). Because we initially observed that Malt1$^{PM/-}$ animals develop spontaneous systemic inflammation with pathological IFNγ levels in vivo, we investigated IFNγ production after T cell activation in more detail. Increased IFNγ mRNA levels were confirmed by RT-PCR analysis in stimulated *Malt1*$^{PM/-}$ T cells in comparison to *Malt1*$^{+/-}$ and *Malt1*$^{-/-}$ T cells (Figure 6B). The inhibition of RNA synthesis by actinomycin D further revealed an increased half-life of IFNγ mRNA in *Malt1*$^{PM/-}$ T cells and in *Malt1*$^{-/-}$ T cells, indicating that IFNγ mRNA stability is controlled by Malt1 (Figure 6C). Consistent with the enhanced total IFNγ mRNA expression levels in *Malt1*$^{PM/-}$ T cells, we also detected higher IFNγ protein production in *Malt1*$^{PM/-}$ T cells compared to both *Malt1*$^{+/-}$ and *Malt1*$^{-/-}$ T cells (Figure 6D). Finally, by extending the microarray analysis of stimulated T cells to global mRNA expression analysis, we observed high expression of interferon-stimulated genes specifically in *Malt1*$^{PM/-}$ T cells but not *Malt1*$^{-/-}$ T cells, demonstrating that interferon signaling is strongly activated in *Malt1*$^{PM/-}$ T cells (Figure 6E). To define the in vivo role of dysregulated IFNγ expression in *Malt1*$^{PM/-}$ mice, we crossed the Malt1^{PM} allele into an *IFNg*-deficient background. Intriguingly, whereas nine out of ten *Malt1*$^{PM/-}$ littermates in an *IFNg*$^{+/+}$ or *IFNg*$^{+/-}$ background had to be euthanized within 20 weeks of birth because they developed the neuropathology described above, the absence of IFNγ rescued the *Malt1*$^{PM/-}$ mice from neuropathology (Figure 6F), although lymphadenopathy was still present in these animals (Figure 6G).

groups as described in the main text. Expression of three representative genes per group is shown, each obtained from four biological replicates per genotype (mean ± SD, two-tailed unpaired t test).

(B) Real-time PCR analysis of IFNγ transcript levels in naive T cells of the given genotypes after in vitro stimulation with anti-CD3/anti-CD28 for 4 hr. The data show representative results from at least three independent experiments (mean ± SD, two-tailed unpaired t test).

(C) CD4$^+$ T cells from *Malt1*$^{+/-}$ (black line, circles), *Malt1*$^{PM/-}$ (dashed line, squares), and *Malt1*$^{-/-}$ (dotted line, triangles) mice were stimulated with PMA and ionomycin for 4 hr, actinomycin D was added to block mRNA synthesis, and IFNγ transcript levels were measured by quantitative PCR at the indicated time points and normalized to β-actin message (n = 4–5, mean ± SEM, two-tailed unpaired t test results are indicated by gray asterisks for *Malt1*$^{PM/-}$ versus *Malt1*$^{+/-}$ or black asterisks for *Malt1*$^{-/-}$ versus *Malt1*$^{+/-}$).

(D) IFNγ protein levels measured by ELISA in supernatants of naive T cells of *Malt1*$^{+/-}$ (n = 4), *Malt1*$^{PM/-}$ (n = 4), and *Malt1*$^{-/-}$ mice (n = 3) after in vitro stimulation with plate-bound anti-CD3/anti-CD28 for 18 hr (mean ± SEM, two-tailed unpaired t test).

(E) Evaluation of the gene expression profiling experiment as described in (A) showing higher expression of interferon-regulated genes in *Malt1*$^{PM/-}$, but not *Malt1*$^{-/-}$, T cells compared with the *Malt1*$^{+/-}$ T cells.

(F) Ataxia scoring of *Malt1*$^{PM/-}$ (n = 10) and *Malt1*$^{PM/-}$; Ifng$^{-/-}$ mice (n = 5). The mice were 20 weeks of age or younger in the case of moribund atactic *Malt1*$^{PM/-}$ animals (mean ± SEM, Mann-Whitney test).

(G) Cells from cervical lymph nodes of *Malt1*$^{+/-}$, *Malt1*$^{PM/-}$, and *Malt1*$^{PM/-}$;*IFNg*$^{-/-}$ mice at 20 weeks of age were stained for lymphocyte populations and analyzed by flow cytometry. The bar graph shows total numbers of B and T cells (n = 4, mean ± SEM).

(H) TNF levels in the serum of *Malt1*$^{+/-}$ (n = 7), *Malt1*$^{PM/-}$ (n = 7), and *Malt1*$^{PM/-}$;*IFNg*$^{-/-}$ mice (n = 8) at an age between 11 and 15 weeks (mean ± SEM, two-tailed unpaired t test).

(I) Body weights for female and male *Malt1*$^{+/-}$, *Malt1*$^{PM/-}$, and *Malt1*$^{PM/-}$;*IFNg*$^{-/-}$ mice at 14–15 weeks of age (mean ± SEM, two-tailed unpaired t test).

(J) Histopathological inflammation scores of gastric antrum tissue samples from *Malt1*$^{+/-}$ (n = 7), *Malt1*$^{PM/-}$ (n = 6), and *Malt1*$^{PM/-}$;*IFNg*$^{-/-}$ mice (n = 5) at 20 weeks of age. Horizontal bars indicate the mean ± SEM (Mann-Whitney test). If not stated otherwise, analyses were performed with animals at 8 to 10 weeks of age. *$p < 0.05$; ns, not significant.

Measurement of inflammatory cytokine concentrations in their serum revealed that the absence of IFNγ led to a significant reduction of TNF concentrations (Figure 6H), and *Malt1*$^{PM/-}$;*IFNg*$^{-/-}$ animals also failed to develop cachexia (Figure 6I). Moreover, the inflammatory activity in the gastric mucosa in *Malt1*$^{PM/-}$;*IFNg*$^{-/-}$ mice was also significantly reduced compared to that in *Malt1*$^{PM/-}$ mice (Figure 6J). Together, these data demonstrate that IFNγ is a key driver of the systemic inflammatory disorder in paracaspase mutant mice.

DISCUSSION

Together, our genetic results identify distinct molecular and cellular functions of Malt1 that act in concert to maintain tissue homeostasis. Together with previously published work, we propose the following model: the Malt1 scaffold sets a threshold for antigen receptor signaling to activate IKK, Jnk, and p38 for proinflammatory gene transcription. The proteolytic activity of Malt1 has a subsequent dual modulatory role: it degrades a series of negative NF-κB regulators to enforce transcription of a subset of immune response genes, and it inactivates an entire class of mRNA-binding proteins that directly control mRNA decay. Thus, both transcriptional activity and mRNA stability, which in combination are highly important for the balanced expression of immune regulatory factors (Ivanov and Anderson, 2013; Villarino et al., 2011), are intimately controlled by the Malt1 protease. These mechanisms differentially control lymphocyte differentiation and activation.

Comparable to a complete Malt1 deletion, the selective inactivation of Malt1 proteolytic activity prevents the development of anti-inflammatory thymus-derived Tregs and of marginal zone and B1 B cells. Although mRNA stability pathways can contribute to developmental lymphocyte fate decisions, the development of these specific T- and B cell lineages is particularly sensitive to perturbations in NF-κB activity (Gerondakis and Siebenlist, 2010). In particular, c-Rel activity is required for regulatory T cell lineage commitment (Ruan et al., 2009). Because the Malt1 protease mediates full NF-κB and c-Rel activation, we hypothesize that such signals are important for the differentiation and/or maintenance of Tregs, marginal zone and B1 B cells.

In contrast to its vital function in lymphocyte development, the paracaspase activity of Malt1 is to a considerable extent dispensable for its mediation of lymphocyte activation. In vitro, T cell signaling induces normal IKK, Jnk, and p38 activation as well as p65 DNA binding and Atf2 phosphorylation, and activated *Malt1*$^{PM/-}$ T cells expand almost as robustly as wild-type T cells. In vivo, the pure Malt1 scaffold is also sufficient to overcome the threshold for productive lymphocyte activation, as demonstrated by the ability of *Malt1*$^{PM/-}$ mice to mount robust adaptive immune responses after T cell-dependent antigen challenge in contrast to *Malt1*$^{-/-}$ animals. However, without Malt1-dependent proteolysis, lymphocyte activity is not appropriately counterbalanced. This can in part be explained by the developmental defects in the Treg lineage, because Tregs are required to prevent lethal multiorgan autoimmune inflammation. Such pathologies occur in the IPEX syndrome, which is caused by a naturally occurring Foxp3 mutation in humans resulting in Treg deficiencies, as well as upon targeted Foxp3 gene inactivation or after toxin-mediated depletion of Tregs in mice (Bacchetta et al., 2006; Kim et al., 2007). Thus, insufficient Treg-dependent suppression of *Malt1*$^{PM/-}$ effector T cells likely supports the pathological accumulation of lymphocytes in paracaspase mutant mice that infiltrate mucosal tissue and drive lethal autoimmune inflammation. Intriguingly, we also observed lymphocyte-dependent degeneration of Purkinje cells in paracaspase mutant mice resulting in a severe cerebellar ataxic syndrome. Although the exact pathomechanism that provokes this neurodegenerative disease remains to be determined, the disorder shares histopathological characteristics with paraneoplastic cerebellar degeneration in human Hodgkin and non-Hodgkin lymphoma, wherein a loss of Purkinje cells is also mediated by aberrant lymphocyte activity (Briani et al., 2011; Darnell, 2004). The inability of lymphocytes that completely lack Malt1 to overcome the initial threshold for activation can explain why these immune-mediated pathologies are observed in *Malt1*$^{PM/-}$ mice, but not in *Malt1*$^{-/-}$ mice.

After activation of conventional T cells, Malt1 not only regulates the NF-κB pathway but also cleaves Roquin-1, Roquin-2, and Regnase-1, which fine-tune the expression of a vast set of target mRNAs, particularly ones that have highly dynamic expression that needs to be altered rapidly during immune responses (Akira, 2013; Jeltsch et al., 2014), and during helper T cell differentiation, Roquin and Regnase-1 cooperate in the repression of shared target mRNAs (Jeltsch et al., 2014). Conditional gene targeting of the individual factors in T cells has shown that Roquin-1, Roquin-2, and Regnase-1 are all required for the maintenance of immune homeostasis (Uehata et al., 2013; Vogel et al., 2013). Transgenic T cell-specific overexpression of Roquin-1 has also been linked to inflammatory responses via enhanced production of IFNγ and other inflammatory cytokines (Ji et al., 2012; Kim et al., 2012). Germline mutations in Roquin-1 that generate hypomorphic Roquin-1 (san) alleles also induce an accumulation of pathological effector T cells with excessive production of IFNγ due to a breakdown in *IFNg* mRNA repression (Chang et al., 2012; Lee et al., 2012; Vinuesa et al., 2005). Thus, nonphysiological levels and activity of Roquin proteins have previously been associated with exacerbated IFNγ production, although the exact molecular mechanisms for this effect have remained unclear. Roquin-1, Roquin-2, and Regnase-1 bind to stem loop motifs of multiple target mRNAs (Akira, 2013), and bioinformatic analysis has estimated that more than 50% of the total transcriptomic changes that are detected during T cell activation are directly regulated at the level of mRNA stability (Cheadle et al., 2005). In addition, Regnase-1 controls gene transcription by directly counteracting the endonuclease Dicer during pre-microRNA processing (Suzuki et al., 2011), and Roquins can also function as degradative ubiquitin ligases for signaling proteins under certain conditions (Maruyama et al., 2014). Thus, in activated *Malt1*$^{PM/-}$ T cells, multiple factors that are primarily controlled by NF-κB, Regnase-1, and Roquin-1 and Roquin-2 are dysregulated and additional genes are assumed to be up- or downregulated secondarily to the primary factors. We observed that the stability of the Regnase-1 and Roquin targets IL-2 and Ox40, but not that of Icos or c-Rel, is diminished in *Malt1*$^{PM/-}$ T cells (data not shown) (Uehata et al., 2013;

Vogel et al., 2013). This overall complexity indicates that more than a single linear pathway is likely responsible for the initiation and perpetuation of the pathological activities of *Malt1*$^{PM/-}$ lymphocytes, and future studies are required to dissect these pathways. Nevertheless, as the final consequence of paracaspase inhibition, we detected excessive IFNγ generation in vivo, and the ability of an *IFNg*$^{-/-}$ background to rescue paracaspase mutant animals from cachexia and neurodegeneration established excessive IFNγ production as a mechanism of the pathology.

Malt1 was originally identified from a chromosomal translocation breakpoint in MALT lymphoma (Dierlamm et al., 1999). Intensive research over more than a decade has identified Malt1 as a major activator of adaptive immunity that can drive normal and malignant lymphocyte proliferation and survival. The overarching paradigm presumes that Malt1 paracaspase inhibition would be immunosuppressive. We report here that Malt1 not only induces and amplifies immune-activating signals but also antagonizes inflammation through its proteolytic activity, which controls regulatory T cell development and intrinsic effector cell pathways of transcription and posttranscriptional regulation. Thus, the distinct threshold and modulatory functions within Malt1 balance pro- and anti-inflammatory immunity. The net outcome of selective paracaspase inactivation in vivo is an imbalance of the immune system that results in lethal lymphocyte- and IFNγ-mediated inflammation. These surprising results cast some concern on the idea of chronically and systemically inhibiting Malt1 proteolytic activity for therapeutic purposes in humans.

EXPERIMENTAL PROCEDURES

Ethics Statement

All animal work was conducted in accordance with German Federal Animal Protection Laws and approved by the Institutional Animal Care and Use Committee at the Technical University of Munich.

Malt1 Paracaspase Enzymatic Assay

Lymphocytes were isolated from spleen and lymph nodes, and 8×10^7 cells were left unstimulated or were stimulated for 30 min at 37°C with 200 nM PMA plus 500 nM ionomycin. The assay was performed as described previously (Nagel et al., 2012).

Serum Cytokine Detection

ELISA was performed using the Mouse IFNγ OptEIA Kit (#555138, BD Biosciences). For detection of serum cytokine concentrations, the Enhanced Sensitivity CBA kit (BD Biosciences) was applied for the respective cytokines.

Neurophenotyping

Ataxia was scored according to a composite phenotyping system including hindlimb clasping, ledge test, gait, and kyphosis as described previously (Guyenet et al., 2010). For rotarod analysis, the mice were tested in ten consecutive trials with 60 s intertrial intervals at constant speed (25 rpm) for a maximum of 120 s per trial on a mouse rotarod (Ugo Basile).

Purification and Stimulation of T Cells

Total T cells were purified by negative selection using magnetic beads (Dynal, Invitrogen) against B cells (B220) and myeloid cells (CD11b). $CD4^+$ T cells were purified using MACS $CD4^+$ or $CD4^+CD62L^+$ T Cell isolation kits (Miltenyi). For cleavage experiments, cells were pretreated with 10 μg/ml MG132 for 20 min at 37°C in medium. Cells were stimulated with PMA (100 nM, Adipogen) and ionomycin (250 nM, Alexis) or with plate-bound anti-CD3 (50 or 5,000 ng/ml, 145-2C11) and anti-CD28 (2 μg/ml, 37.51, both from eBioscience) antibodies after precoating with anti-Syrian hamster antibodies (10 μg/ml, F[ab′]2 fragment of IgG H^+L, rabbit, Jackson ImmunoResearch) in RPMI 1640 medium supplemented with 5% fetal bovine serum (v/v), penicillin (100 U/ml)/streptomycin (100 μg/ml), L-glutamine (2 mM), and 2-mercaptoethanol (50 μM, all Gibco) for the indicated time points at 37°C.

Statistics

Statistical analysis was performed using GraphPad Prism (GraphPad Software) and Microsoft Excel. In general, groups were compared using unpaired two-tailed t tests assuming normal distributions and unequal variances or unpaired two-tailed Mann-Whitney tests as indicated in the figure legends.

ACCESSION NUMBERS

The gene expression profiling raw data that were used for analyses in this paper have been uploaded to the NCBI Gene Expression Omnibus under the accession number GSE55360.

SUPPLEMENTAL INFORMATION

Supplemental Information includes Supplemental Experimental Procedures and three figures and can be found with this article online at http://dx.doi.org/10.1016/j.celrep.2014.10.044.

AUTHOR CONTRIBUTIONS

A.G., O.G., and J.R. designed the Study. All authors designed and performed experiments. All authors analyzed the results. A.G., O.G., and J.R. designed the figures and wrote the paper.

ACKNOWLEDGMENTS

We thank Lisa Bartnik, Sabrina Krebs, Tanja Ruff, Markus Utzt, Nicole Hannesschläger, Daniel Nagel, Desiree Argiriu, and Anke Bettenbrock for technical assistance, Beatrix Lunk and the ZPF animal facility team for excellent mouse care, and Susanne Roth, Nathalie Knies, and Daniel Krappmann for critical discussions. This work was supported by the Preclinical Comprehensive Cancer Center (PCCC) of the Helmholtz Alliance to W.Weichert, an Intrafrontier Grant (01KX1012) to J.B., the EUCOMMTOOLS project supported by the European Commission (FP7-HEALTH-F4-2010-261492) to W. Wurst, a Heisenberg award from the Deutsche Forschungsgemeinschaft (DFG; KO2964/3-2), DFG grants (SFB1054 and TR128) and SyNergy (Munich Cluster for Systems Neurology) to T.K., an SFB grant (1054 TP A03) from DFG and an ERC Starting Grant to V.H., the Preclinical Comprehensive Cancer Center (PCCC) of the Helmholtz Alliance, the Helmholtz Foundation, an ERC Starting Grant (LiverCancerMechanism) to M. Heikenwalder, SFB grants (SFB 1054, SFB 684, and RU 695/6-1) from the DFG, and by ERC Advanced Grant from the European Research Council under the European Union's Seventh Framework Programme (FP7/2007-2013)/ERC grant agreement 322865 to J.R.

Received: May 16, 2014
Revised: September 15, 2014
Accepted: October 15, 2014
Published: November 13, 2014

REFERENCES

Akagi, T., Motegi, M., Tamura, A., Suzuki, R., Hosokawa, Y., Suzuki, H., Ota, H., Nakamura, S., Morishima, Y., Taniwaki, M., and Seto, M. (1999). A novel gene, MALT1 at 18q21, is involved in t(11;18) (q21;q21) found in low-grade B-cell lymphoma of mucosa-associated lymphoid tissue. Oncogene *18*, 5785–5794.

Akira, S. (2013). Regnase-1, a ribonuclease involved in the regulation of immune responses. Cold Spring Harb. Symp. Quant. Biol. *78*, 51–60.

Bacchetta, R., Passerini, L., Gambineri, E., Dai, M., Allan, S.E., Perroni, L., Dagna-Bricarelli, F., Sartirana, C., Matthes-Martin, S., Lawitschka, A., et al.

(2006). Defective regulatory and effector T cell functions in patients with FOXP3 mutations. J. Clin. Invest. *116*, 1713–1722.

Briani, C., Vitaliani, R., Grisold, W., Honnorat, J., Graus, F., Antoine, J.C., Bertolini, G., and Giometto, B.; PNS Euronetwork (2011). Spectrum of paraneoplastic disease associated with lymphoma. Neurology *76*, 705–710.

Brüstle, A., Brenner, D., Knobbe, C.B., Lang, P.A., Virtanen, C., Hershenfield, B.M., Reardon, C., Lacher, S.M., Ruland, J., Ohashi, P.S., and Mak, T.W. (2012). The NF-κB regulator MALT1 determines the encephalitogenic potential of Th17 cells. J. Clin. Invest. *122*, 4698–4709.

Chang, P.P., Lee, S.K., Hu, X., Davey, G., Duan, G., Cho, J.H., Karupiah, G., Sprent, J., Heath, W.R., Bertram, E.M., and Vinuesa, C.G. (2012). Breakdown in repression of IFN-γ mRNA leads to accumulation of self-reactive effector CD8+ T cells. J. Immunol. *189*, 701–710.

Cheadle, C., Fan, J., Cho-Chung, Y.S., Werner, T., Ray, J., Do, L., Gorospe, M., and Becker, K.G. (2005). Stability regulation of mRNA and the control of gene expression. Ann. N Y Acad. Sci. *1058*, 196–204.

Coornaert, B., Baens, M., Heyninck, K., Bekaert, T., Haegman, M., Staal, J., Sun, L., Chen, Z.J., Marynen, P., and Beyaert, R. (2008). T cell antigen receptor stimulation induces MALT1 paracaspase-mediated cleavage of the NF-kappaB inhibitor A20. Nat. Immunol. *9*, 263–271.

Darnell, R.B. (2004). Paraneoplastic neurologic disorders: windows into neuronal function and tumor immunity. Arch. Neurol. *61*, 30–32.

Dierlamm, J., Baens, M., Wlodarska, I., Stefanova-Ouzounova, M., Hernandez, J.M., Hossfeld, D.K., De Wolf-Peeters, C., Hagemeijer, A., Van den Berghe, H., and Marynen, P. (1999). The apoptosis inhibitor gene API2 and a novel 18q gene, MLT, are recurrently rearranged in the t(11;18)(q21;q21) associated with mucosa-associated lymphoid tissue lymphomas. Blood *93*, 3601–3609.

Düwel, M., Hadian, K., and Krappmann, D. (2010). Ubiquitin Conjugation and Deconjugation in NF-κB Signaling. Subcell. Biochem. *54*, 88–99.

Ferch, U., Kloo, B., Gewies, A., Pfänder, V., Düwel, M., Peschel, C., Krappmann, D., and Ruland, J. (2009). Inhibition of MALT1 protease activity is selectively toxic for activated B cell-like diffuse large B cell lymphoma cells. J. Exp. Med. *206*, 2313–2320.

Fontán, L., and Melnick, A. (2013). Molecular pathways: targeting MALT1 paracaspase activity in lymphoma. Clin. Cancer Res. *19*, 6662–6668.

Gerondakis, S., and Siebenlist, U. (2010). Roles of the NF-kappaB pathway in lymphocyte development and function. Cold Spring Harb. Perspect. Biol. *2*, a000182.

Gozdecka, M., and Breitwieser, W. (2012). The roles of ATF2 (activating transcription factor 2) in tumorigenesis. Biochem. Soc. Trans. *40*, 230–234.

Greil, J., Rausch, T., Giese, T., Bandapalli, O.R., Daniel, V., Bekeredjian-Ding, I., Stütz, A.M., Drees, C., Roth, S., Ruland, J., et al. (2013). Whole-exome sequencing links caspase recruitment domain 11 (CARD11) inactivation to severe combined immunodeficiency. J. Allergy Clin. Immunol. *131*, 1376–1383.e3.

Guyenet, S.J., Furrer, S.A., Damian, V.M., Baughan, T.D., La Spada, A.R., and Garden, G.A. (2010). A simple composite phenotype scoring system for evaluating mouse models of cerebellar ataxia. J. Vis. Exp.

Hailfinger, S., Nogai, H., Pelzer, C., Jaworski, M., Cabalzar, K., Charton, J.E., Guzzardi, M., Décaillet, C., Grau, M., Dörken, B., et al. (2011). Malt1-dependent RelB cleavage promotes canonical NF-kappaB activation in lymphocytes and lymphoma cell lines. Proc. Natl. Acad. Sci. USA *108*, 14596–14601.

Ivanov, P., and Anderson, P. (2013). Post-transcriptional regulatory networks in immunity. Immunol. Rev. *253*, 253–272.

Jabara, H.H., Ohsumi, T., Chou, J., Massaad, M.J., Benson, H., Megarbane, A., Chouery, E., Mikhael, R., Gorka, O., Gewies, A., et al. (2013). A homozygous mucosa-associated lymphoid tissue 1 (MALT1) mutation in a family with combined immunodeficiency. J. Allergy Clin. Immunol. *132*, 151–158.

Jeltsch, K.M., Hu, D., Brenner, S., Zöller, J., Heinz, G.A., Nagel, D., Vogel, K.U., Rehage, N., Warth, S.C., Edelmann, S.L., et al. (2014). Cleavage of roquin and regnase-1 by the paracaspase MALT1 releases their cooperatively repressed targets to promote TH17 differentiation. Nat. Immunol. *15*, 1079–1089.

Ji, Y.R., Kim, H.J., Yu, D.H., Bae, K.B., Park, S.J., Yi, J.K., Kim, N., Park, S.J., Oh, K.B., Hwang, S.S., et al. (2012). Enforced expression of roquin protein in T cells exacerbates the incidence and severity of experimental arthritis. J. Biol. Chem. *287*, 42269–42277.

Kim, J.M., Rasmussen, J.P., and Rudensky, A.Y. (2007). Regulatory T cells prevent catastrophic autoimmunity throughout the lifespan of mice. Nat. Immunol. *8*, 191–197.

Kim, H.J., Ji, Y.R., Kim, M.O., Yu, D.H., Shin, M.J., Yuh, H.S., Bae, K.B., Park, Sj., Yi, J.K., Kim, N.R., et al. (2012). The role of Roquin overexpression in the modulation of signaling during in vitro and ex vivo T-cell activation. Biochem. Biophys. Res. Commun. *417*, 280–286.

Kullmann, J.A., Neumeyer, A., Wickertsheim, I., Böttcher, R.T., Costell, M., Deitmer, J.W., Witke, W., Friauf, E., and Rust, M.B. (2012). Purkinje cell loss and motor coordination defects in profilin1 mutant mice. Neuroscience *223*, 355–364.

Lee, S.K., Silva, D.G., Martin, J.L., Pratama, A., Hu, X., Chang, P.P., Walters, G., and Vinuesa, C.G. (2012). Interferon-γ excess leads to pathogenic accumulation of follicular helper T cells and germinal centers. Immunity *37*, 880–892.

Lenz, G., Davis, R.E., Ngo, V.N., Lam, L., George, T.C., Wright, G.W., Dave, S.S., Zhao, H., Xu, W., Rosenwald, A., et al. (2008). Oncogenic CARD11 mutations in human diffuse large B cell lymphoma. Science *319*, 1676–1679.

Leppek, K., Schott, J., Reitter, S., Poetz, F., Hammond, M.C., and Stoecklin, G. (2013). Roquin promotes constitutive mRNA decay via a conserved class of stem-loop recognition motifs. Cell *153*, 869–881.

Maruyama, T., Araki, T., Kawarazaki, Y., Naguro, I., Heynen, S., Aza-Blanc, P., Ronai, Z., Matsuzawa, A., and Ichijo, H. (2014). Roquin-2 promotes ubiquitin-mediated degradation of ASK1 to regulate stress responses. Sci. Signal. *7*, ra8.

McKinnon, M.L., Rozmus, J., Fung, S.Y., Hirschfeld, A.F., Del Bel, K.L., Thomas, L., Marr, N., Martin, S.D., Marwaha, A.K., Priatel, J.J., et al. (2014). Combined immunodeficiency associated with homozygous MALT1 mutations. J. Allergy Clin. Immunol. *133*, 1458–1462, e1–e7.

Nagel, D., Spranger, S., Vincendeau, M., Grau, M., Raffegerst, S., Kloo, B., Hlahla, D., Neuenschwander, M., Peter von Kries, J., Hadian, K., et al. (2012). Pharmacologic inhibition of MALT1 protease by phenothiazines as a therapeutic approach for the treatment of aggressive ABC-DLBCL. Cancer Cell *22*, 825–837.

Newton, K., and Dixit, V.M. (2003). Mice lacking the CARD of CARMA1 exhibit defective B lymphocyte development and impaired proliferation of their B and T lymphocytes. Curr. Biol. *13*, 1247–1251.

Oh, S.Y., Cho, K.A., Kang, J.L., Kim, K.H., and Woo, S.Y. (2014). Comparison of experimental mouse models of inflammatory bowel disease. Int. J. Mol. Med. *33*, 333–340.

Reiley, W.W., Jin, W., Lee, A.J., Wright, A., Wu, X., Tewalt, E.F., Leonard, T.O., Norbury, C.C., Fitzpatrick, L., Zhang, M., and Sun, S.C. (2007). Deubiquitinating enzyme CYLD negatively regulates the ubiquitin-dependent kinase Tak1 and prevents abnormal T cell responses. J. Exp. Med. *204*, 1475–1485.

Ruan, Q., Kameswaran, V., Tone, Y., Li, L., Liou, H.C., Greene, M.I., Tone, M., and Chen, Y.H. (2009). Development of Foxp3(+) regulatory t cells is driven by the c-Rel enhanceosome. Immunity *31*, 932–940.

Ruefli-Brasse, A.A., French, D.M., and Dixit, V.M. (2003). Regulation of NF-kappaB-dependent lymphocyte activation and development by paracaspase. Science *302*, 1581–1584.

Ruland, J., Duncan, G.S., Elia, A., del Barco Barrantes, I., Nguyen, L., Plyte, S., Millar, D.G., Bouchard, D., Wakeham, A., Ohashi, P.S., and Mak, T.W. (2001). Bcl10 is a positive regulator of antigen receptor-induced activation of NF-kappaB and neural tube closure. Cell *104*, 33–42.

Ruland, J., Duncan, G.S., Wakeham, A., and Mak, T.W. (2003). Differential requirement for Malt1 in T and B cell antigen receptor signaling. Immunity *19*, 749–758.

Shiotsuki, H., Yoshimi, K., Shimo, Y., Funayama, M., Takamatsu, Y., Ikeda, K., Takahashi, R., Kitazawa, S., and Hattori, N. (2010). A rotarod test for evaluation of motor skill learning. J. Neurosci. Methods *189*, 180–185.

Staal, J., Driege, Y., Bekaert, T., Demeyer, A., Muyllaert, D., Van Damme, P., Gevaert, K., and Beyaert, R. (2011). T-cell receptor-induced JNK activation requires proteolytic inactivation of CYLD by MALT1. EMBO J. *30*, 1742–1752.

Staudt, L.M. (2010). Oncogenic activation of NF-kappaB. Cold Spring Harb. Perspect. Biol. *2*, a000109.

Streubel, B., Lamprecht, A., Dierlamm, J., Cerroni, L., Stolte, M., Ott, G., Raderer, M., and Chott, A. (2003). T(14;18)(q32;q21) involving IGH and MALT1 is a frequent chromosomal aberration in MALT lymphoma. Blood *101*, 2335–2339.

Suzuki, H.I., Arase, M., Matsuyama, H., Choi, Y.L., Ueno, T., Mano, H., Sugimoto, K., and Miyazono, K. (2011). MCPIP1 ribonuclease antagonizes dicer and terminates microRNA biogenesis through precursor microRNA degradation. Mol. Cell *44*, 424–436.

Thome, M., Charton, J.E., Pelzer, C., and Hailfinger, S. (2010). Antigen receptor signaling to NF-kappaB via CARMA1, BCL10, and MALT1. Cold Spring Harb. Perspect. Biol. *2*, a003004.

Uehata, T., Iwasaki, H., Vandenbon, A., Matsushita, K., Hernandez-Cuellar, E., Kuniyoshi, K., Satoh, T., Mino, T., Suzuki, Y., Standley, D.M., et al. (2013). Malt1-induced cleavage of regnase-1 in CD4(+) helper T cells regulates immune activation. Cell *153*, 1036–1049.

Villarino, A.V., Katzman, S.D., Gallo, E., Miller, O., Jiang, S., McManus, M.T., and Abbas, A.K. (2011). Posttranscriptional silencing of effector cytokine mRNA underlies the anergic phenotype of self-reactive T cells. Immunity *34*, 50–60.

Vinuesa, C.G., Cook, M.C., Angelucci, C., Athanasopoulos, V., Rui, L., Hill, K.M., Yu, D., Domaschenz, H., Whittle, B., Lambe, T., et al. (2005). A RING-type ubiquitin ligase family member required to repress follicular helper T cells and autoimmunity. Nature *435*, 452–458.

Vogel, K.U., Edelmann, S.L., Jeltsch, K.M., Bertossi, A., Heger, K., Heinz, G.A., Zöller, J., Warth, S.C., Hoefig, K.P., Lohs, C., et al. (2013). Roquin paralogs 1 and 2 redundantly repress the Icos and Ox40 costimulator mRNAs and control follicular helper T cell differentiation. Immunity *38*, 655–668.

Vucic, D., and Dixit, V.M. (2009). Masking MALT1: the paracaspase's potential for cancer therapy. J. Exp. Med. *206*, 2309–2312.

Willis, T.G., Jadayel, D.M., Du, M.Q., Peng, H., Perry, A.R., Abdul-Rauf, M., Price, H., Karran, L., Majekodunmi, O., Wlodarska, I., et al. (1999). Bcl10 is involved in t(1;14)(p22;q32) of MALT B cell lymphoma and mutated in multiple tumor types. Cell *96*, 35–45.

Cell Reports, Volume *9*

Supplemental Information

Uncoupling Malt1 Threshold Function from Paracaspase Activity Results in Destructive Autoimmune Inflammation

Andreas Gewies, Oliver Gorka, Hanna Bergmann, Konstanze Pechloff, Franziska Petermann, Katharina M. Jeltsch, Martina Rudelius, Mark Kriegsmann, Wilko Weichert, Marion Horsch, Johannes Beckers, Wolfgang Wurst, Mathias Heikenwalder, Thomas Korn, Vigo Heissmeyer, and Jürgen Ruland

Inventory of Supplemental Information

Supplemental information include three supplemental figures (Figures S1–S3), Supplemental Experimental Procedures and Supplemental References.

Figure S1
Generation of Malt1 paracaspase mutant mice.
Related to Supplemental Experimental Procedure “Generation of *Malt1* paracaspase mutant (PM) knock-in mice”

Figure S2
Phenotypic analysis of *Malt1*$^{PM/-}$, *Malt1*$^{PM/PM}$ and *Malt1*$^{PM/+}$ animals.
Related to Fig. 1

Figure S3
Cleavage of Malt1 targets in T cells from *Malt1*$^{+/-}$, *Malt1*$^{PM/-}$ and *Malt1*$^{-/-}$ mice.
Related to Fig. 5

Supplemental Experimental Procedures

Supplemental References

Figure S1

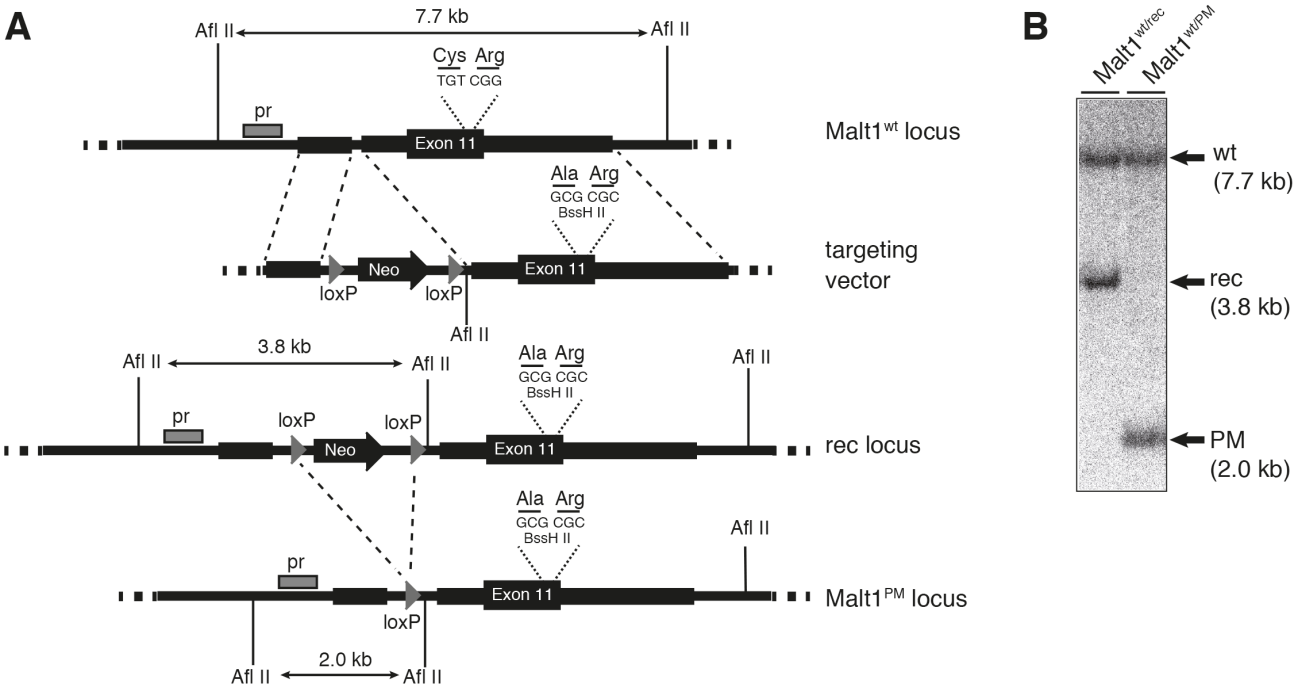

Figure S1 -
related to Supplemental Experimental Procedure "Generation of *Malt1* paracaspase mutant (PM) knock-in mice":

Generation of Malt1 paracaspase mutant mice. (A) Targeting strategy for homologous recombination at the *Malt1* genomic locus. The exon 11 region is shown, indicating the restriction fragment lengths produced by Afl II in the wild-type (wt), recombinant (rec), or PM allele that could be analyzed by Southern blotting using the probe (pr) marked in grey. The targeting vector contains the terminal homology arms indicated by thick lines, exon 11 with the cysteine (TGT) to alanine (GCG) mutation in codon 472 and a silent mutation in codon 473 (CGG → CGC) generating an artificial BssH II site. The neomycin (Neo) selection cassette is flanked by loxP sites (grey triangles). Homologous recombination in ES cells produced the rec locus containing the mutated exon 11 and the loxP flanked Neo cassette. Crossing the rec allele in mice to cre deleter mice led to the removal of the Neo cassette and thus to the generation of the PM allele. **(B)** Southern blot validation of the wild-type (wt), recombinant (rec), and paracaspase mutant (PM) Malt1 alleles generated by homologous recombination of the *Malt1* locus. AflII-digested genomic DNA isolated from *Malt1*$^{wt/rec}$ thymi demonstrated the presence of the expected 7.7-kb wt fragment and the 3.8-kb rec fragment. Deletion of the neomycin (Neo) resistance cassette yielded the *Malt1*$^{wt/PM}$ genotype (also named *Malt1*$^{PM/+}$ within this manuscript) which was confirmed by detecting the expected PM fragment at 2.0 kb.

Figure S2

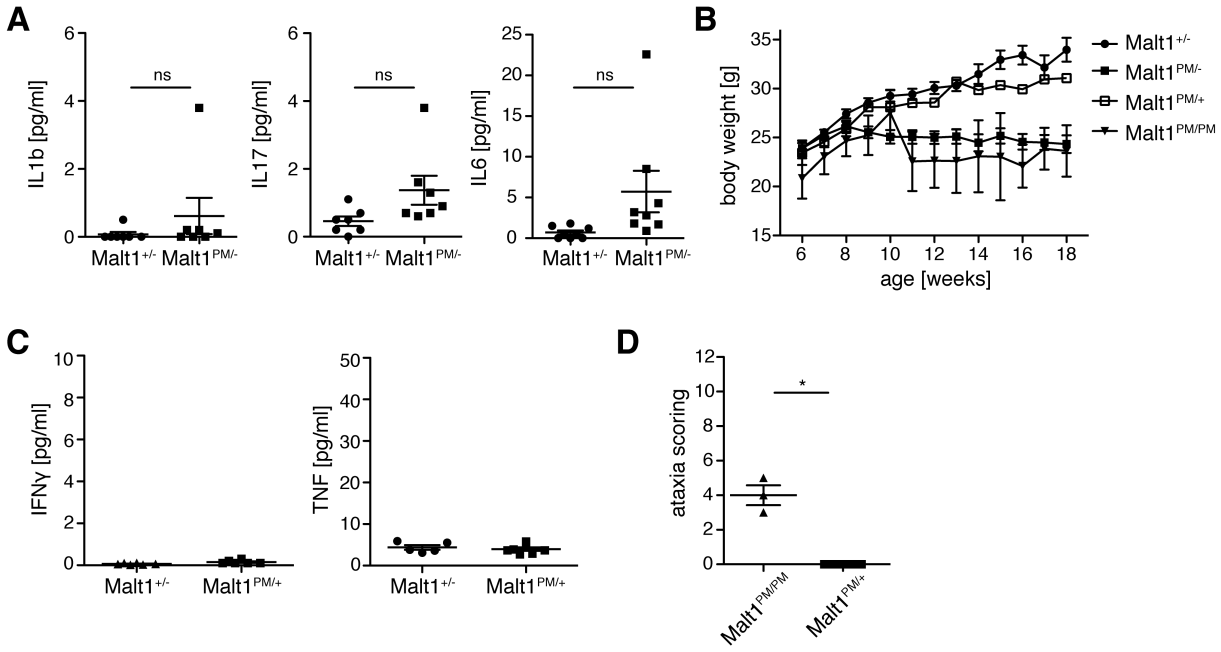

Figure S2 –
related to Fig. 1:

Phenotypic analysis of *Malt1*$^{PM/-}$, *Malt1*$^{PM/PM}$ and *Malt1*$^{PM/+}$ animals. (A) Serum concentrations of IL-1β, IL-17, and IL-6 were measured for *Malt1*$^{+/-}$ (n=7) and *Malt1*$^{PM/-}$ (n=7-8) mice at an age of 6 to 10 weeks. Horizontal bars indicate the means ± SEM (two-tailed unpaired t-test). **(B)** Body weight curves for *Malt1*$^{PM/+}$ and *Malt1*$^{PM/PM}$ mice were compared to those of *Malt1*$^{+/-}$ and *Malt1*$^{PM/-}$ mice (n>3 per time point, means ± SEM). **(C)** IFNγ and TNF levels in the serum of *Malt1*$^{+/-}$ (n=5) and *Malt1*$^{PM/+}$ (n=5) animals at 3-5 months of age. Horizontal bars indicate the means ± SEM (two-tailed unpaired t-test). **(D)** Ataxia scoring of *Malt1*$^{PM/PM}$ (n=3), and *Malt1*$^{PM/+}$ (n=6) at an age of 4 -5 months. Horizontal bars indicate the means ± SEM, Mann-Whitney test. * $P < 0.05$, ns = not significant.

Figure S3

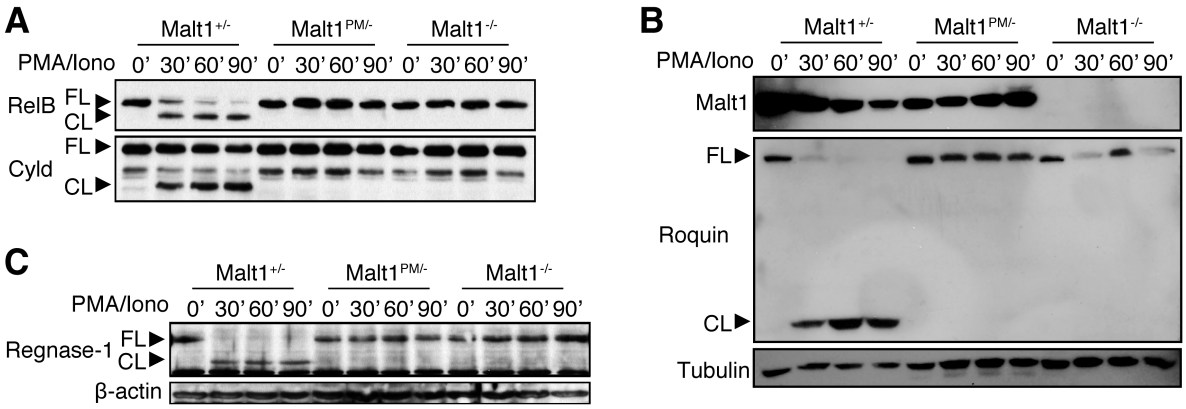

Figure S3 –
related to Fig. 5:

Cleavage of Malt1 targets in T cells from *Malt1*$^{+/-}$, *Malt1*$^{PM/-}$ and *Malt1*$^{-/-}$ mice. (A) CD4+ T cells from *Malt1*$^{+/-}$, *Malt1*$^{PM/-}$, and *Malt1*$^{-/-}$ mice were stimulated with PMA and ionomycin for the indicated time points in the presence of the proteasome inhibitor MG132. Cell lysates were analyzed by immunoblot using antibodies to RelB and Cyld. **(B, C)** CD4+ T cells from *Malt1*$^{+/-}$, *Malt1*$^{PM/-}$, and *Malt1*$^{-/-}$ mice were stimulated as in (A) and analyzed by immunoblot using specific antibodies to Malt1, Roquin1/2, and tubulin (B) or Regnase-1 and β-actin (C).

Supplemental Experimental Procedures

Generation of *Malt1* paracaspase mutant (PM) knock-in mice. A 715 bp fragment within intron 10 of the *Malt1* gene was used as a short arm (SA) for homologous recombination, and a 5.6 kb sequence downstream of the SA including exon 11 with the mutated nucleotide stretch TGTCGG (Cys-Arg) → GCGCGC (Ala-Arg) at codons 472+473 was used as a long arm (LA) for homologous recombination (see Figure S1 A). SA and LA were cloned into the pSPUC-DTA targeting vector which then was electroporated into E14tg2A.4 ES cells according to standard procedures. Cre deleter mice (Jax human CMV-Cre deleter strain B6.C-Tg(CMV-cre)1Cgn/J) were used to remove the Neo cassette. The *Malt1*^{PM} allele was back crossed to the C57bl/6J background for at least 8 generations (N8), all other mouse strains used in this study were also in a C57bl/6 background. *Malt1*$^{PM/+}$ mice were crossed with *Malt1*$^{-/-}$ mice (Ruland et al., 2003) to compare mice with a paracaspase mutant allele (Malt1$^{PM/-}$) to control animals with wt Malt1 (*Malt1*$^{+/-}$) or to Malt1-deficient (*Malt1*$^{-/-}$) mice. As indicated in the text, the *Malt1*$^{PM/-}$ alleles were also crossed to *Bcl10*$^{-/-}$ mice (Ruland et al., 2001), *Rag1*$^{-/-}$ mice (B6.129S7-Rag1^{tm1Mom}/J) and *IFNg*$^{-/-}$ mice (B6.129S7-Ifng^{tm1Ts}/J). Mice were housed in a specific pathogen-free facility according to the FELASA recommendations (http://www.felasa.eu).

Genotyping PCR and Southern blotting. To distinguish the wild-type *Malt1* paracaspase allele from the PM allele, the following primers were used: fwd: 5'-ctggtggcacacactttag -3' and rev: 5'-ccaacatacatacgaatggac-3', which produce a 160 bp band for the paracaspase wt allele and a 340 bp band for the PM allele. To distinguish the *Malt1* wt from the ko (-) allele, the following primer set was used: fwd: 5'-actttcatcttgccagcactctttctta-3', wt rev: 5'-ctgctgctgacatgctacaatatgctg-3' or ko rev: 5'-gggtgggattagataaatgcctgctc, which produce a 500 bp band for the wt allele and a 400 bp band for the knockout allele. Southern hybridization was performed according to standard protocols.

Flow cytometry. To quantify cell populations by flow cytometry, single cell suspensions were stained with fluorochrome-labeled antibodies directed against CD4

(GK1.5), CD8a (53-6.7), B220 (RA3-6B2), CD19 (eBio1D3), TCRβ (H57-597), IgM (II/41), CD21 (7G6), CD23 (B3B4), CD25 (PC61.5), CD62L (MEL-14), CD44 (IM7), CD69 (H1.2F3), Foxp3 (FJK-16s) and CD16/CD32 (clone 93) all obtained from eBioscience or BD Biosciences. For intracellular staining, cells were fixed and permeabilized with a Foxp3 staining kit (eBioscience). For proliferation assays, MACS-bead purified CD4+ T cells were labeled with 2.5 μM carboxyfluorescein succinimidyl ester (CFSE) for 10 min at 37°C and subsequently incubated for the indicated times at 37°C. For survival assays, cells were stained with Annexin V and 7-AAD in Annexin V staining buffer (both eBioscience). Analyses of cell populations and proliferation were performed by flow cytometry in a FACSCantoII (BD). Immune populations in the brain were determined as described previously (Rothhammer et al., 2011).

Histology and immunohistochemistry. Organs were formalin-fixed, paraffin-embedded and cut (2 μm) before tissue sections were stained with HE. For immunohistochemical staining of Purkinje cells in the cerebella, an anti-calbindin antibody (ab1778, Abcam) was used with the Ventana i-view system. Images were acquired using either an Olympus BX53 microscope and CellSens Dimension Software or an AxioVert (Zeiss) microscope with an AxioCam and processed by AxioVision software (Carl Zeiss). Hematoxylin and eosin (HE) stained gastric tissue sections from all mice were evaluated by a pathologist (MK) according to the updated Sydney classification (Dixon et al., 1996) in order to determine the inflammatory activity in the gastric antrum. Grading of active and chronic inflammation was combined into an overall four-tier semiquantitative score (0=no inflammation, 1=mild inflammation, 2=moderate inflammation, 3=strong inflammation).

DSS colitis. At 8 weeks of age mice were treated with 3.5% DSS in their drinking water for 5 days and sacrificed on day 9 at the peak of colitis. The bodyweights of the animals were monitored daily, and the animals were euthanized if their bodyweights dropped by 20% of the initial body weight. The severity of DSS colitis in the mice was assessed by scoring the most affected area of each mouse from HE-stained formalin-fixed paraffin-embedded colon sections on a scale from 1-12. Scoring was

determined by criteria of immune cell infiltration, edema, epithelial damage and hyperplasia (Okayasu et al., 1990).

Immunization. Eight to nine-week-old mice were immunized intraperitoneally (i.p.) with 200 µl of $KAl(SO_4)_2*12H_2O$ (f.c. 5% (w/v), Sigma) precipitated nitrophenyl (NP)(18) ovalbumin (OVA) (f.c 0.5 mg/ml, Biosearch Technologies). NP-specific serum IgM and IgG1 concentrations were determined by ELISA applying the SBA Clonotyping™ System-AP and Mouse Immunoglobulin Panel (SouthernBiotech).

Immunoblot analysis. Cells were lysed in CHAPS lysis buffer (20 mM Tris·Cl pH 7.5, 150 mM NaCl, 1% CHAPS) after addition of protease inhibitor cocktail (Sigma). Immunoblot analysis was performed according to standard protocols. Antibodies from Cell Signaling
Technology were used to detect p-Erk (#9101), p-JNK (#9251), p-p38 (#9211), p-IKKa/IKKb (#2697), IkBa (#9242), p-IkBa (#9246), RelB (#4922) and p-Atf2 (#5112), otherwise Cyld (E-10, Santa Cruz), Regnase-1 (clone 604421**,** R&D), Roquin (clone 3F12 provided by V. Heissmeyer), Malt1 (Ruefli-Brasse et al., 2003), Gapdh (Calbiochem, CB1001), b-actin (A5060, Sigma) and Tubulin (sc-23948, Santa Cruz) were used.

NF-κB assays. Electromobility shift assays were performed as described (Ruland et al., 2001) and ELISA-based NF-κB binding assays were performed with nuclear extracts using the TransAM® NF-κB factor ELISA Kit (Active Motif). To detect p50, p52, RelB and p65 antibodies provided by the TransAM® kit were used; to detect cRel the sc-71 X antibody (Santa Cruz Biotechnology) was used.

qRT PCR analysis and RNA stability assay. For qRT PCR, total RNA was prepared using a combination of TRIzol extraction and subsequent column purification (RNeasy kit, Qiagen). cDNA was synthesized from total RNA using Superscript II Reverse Transcriptase (Life Technologies) with random primers. qPCR was performed using a LightCycler LC480 (Roche) and SYBR green from the qPCR Core kit (Eurogentec). To assay RNA stability, bead-purified CD4+ T-cells were

stimulated for four hours with PMA/ionomycin before transcription was blocked by the addition of actinomycin D (10 µg/ml) for the indicated time points. Total RNA isolation and qPCR were performed as described above. The following primers were used for qPCR: Ifng-fwd: ctgaataactattttaactcaagtg, Ifng-rev: gattttcatgtcaccatccttttg; Tnf-fwd: actccaggcggtgcctatg, Tnf-rev: gagcgtggtggcccct; and as a reference ActB-fwd: cacacccgccaccagttcg, ActB-rev: caccatcacaccctggtgc.

Microarray analysis. Naive CD4+ T cells (CD62L+ CD25-) were sorted using a MoFlo cell sorter (Beckman Coulter) and stimulated with 50 ng/ml plate-bound anti-CD3 (145-2C11) and 2 µg/ml anti-CD28 (37.51) antibodies after pre-coating with anti-Syrian hamster antibodies using a minimum of $3x10^6$ cells per time point in one well of a 6-well plate. Total RNA was isolated as described for the qRT PCR analysis, and the quality was validated by analysis with an Agilent Bioanalyzer. RNA was amplified using the Illumina TotalPrep RNA amplification kit (Ambion). The amplified cRNA was hybridized to MouseRef-8v2 Expression BeadChips (Illumina, San Diego) for 16 h. Staining and scanning were performed according to the Illumina expression protocol. Data were normalized using the GenomeStudio Version 2011.1 software and processed using quantile normalization, the background subtraction option, and the introduction of an offset to remove remaining negative expression values. Statistical analysis was performed with the TM4 software package, selecting significantly regulated genes with a fold change > 2 in combination with a FDR < 10%. The expression profiling data set was submitted to the GEO database (GSE55360, http://www.ncbi.nlm.nih.gov/geo/query/acc.cgi?token=ajsdwguspxcrvkf&acc=GSE55360). NF-kB target genes were defined according to the Gilmore laboratory at Boston University (http://www.bu.edu/nf-kb/gene-resources/target-genes/) and additional previous reports (Compagno et al., 2009).

Supplemental References

Compagno, M., Lim, W.K., Grunn, A., Nandula, S.V., Brahmachary, M., Shen, Q., Bertoni, F., Ponzoni, M., Scandurra, M., Califano, A.*, et al.* (2009). Mutations of multiple genes cause deregulation of NF-kappaB in diffuse large B-cell lymphoma. Nature *459*, 717-721.

Dixon, M.F., Genta, R.M., Yardley, J.H., and Correa, P. (1996). Classification and grading of gastritis. The updated Sydney System. International Workshop on the Histopathology of Gastritis, Houston 1994. The American Journal of Surgical Pathology *20*, 1161-1181.

Okayasu, I., Hatakeyama, S., Yamada, M., Ohkusa, T., Inagaki, Y., and Nakaya, R. (1990). A novel method in the induction of reliable experimental acute and chronic ulcerative colitis in mice. Gastroenterology *98*, 694-702.

Rothhammer, V., Heink, S., Petermann, F., Srivastava, R., Claussen, M.C., Hemmer, B., and Korn, T. (2011). Th17 lymphocytes traffic to the central nervous system independently of alpha4 integrin expression during EAE. The Journal of Experimental Medicine *208*, 2465-2476.